Authors

Adrianus J. Westgeest[1,†], Myriam Dauzat[1], Thierry Simonneau[1], Florent Pantin[1,*, ‡]

*Author for correspondence: florent.pantin@institut-agro.fr

[1]LEPSE, Univ Montpellier, INRAE, Institut Agro, Montpellier, France

[†]Present address: CEFE, Univ Montpellier, CNRS, EPHE, IRD, Montpellier, France

[‡]Present address: IRHS, INRAE, Institut Agro, Université d'Angers, Beaucouzé, France

Title

Leaf starch metabolism sets the phase of stomatal rhythm

Short title

Diel transpiration dynamics and starch

One-sentence summary

The PhenoLeaks pipeline for monitoring diel transpiration dynamics reveals that leaf starch metabolism sets the timing of the endogenous stomatal rhythm.

ABSTRACT

In leaves, stomata open during the day to favour CO_2 entry for photosynthesis, and close at night to prevent inefficient transpiration of water vapour. Plants' days and nights are paced by light availability and anticipated by the circadian clock, but how rhythmic stomatal movements are interlocked with the environment and the physiology of the plant remains elusive. Leaf transitory starch appears as a plausible integrator therein. Here, we developed PhenoLeaks, a pipeline to analyse the diel (24-h) dynamics of transpiration, and used it to screen a series of Arabidopsis mutants impaired in starch metabolism. We show that the diel dynamics of transpiration are driven by a sinusoidal, endogenous rhythm that overarches days and nights. We uncover that a number of severe mutations in starch metabolism affect the endogenous rhythm through a phase shift, resulting in delayed stomatal movements throughout the daytime and reduced stomatal preopening during the night. Nevertheless, analysis of tissue-specific mutations revealed that neither guard-cell nor mesophyll-cell starch metabolism are strictly required for normal diel patterns of transpiration. We propose that leaf starch metabolism affects the endogenous stomatal rhythm by modulating cross-tissue sugar homeostasis, which interacts with the circadian clock that in turn affects guard-cell ion transport.

INTRODUCTION

Leaf stomata are tiny pores surrounded by pairs of guard cells that control carbon gain and water loss in plants (Hetherington and Woodward, 2003). Every day, stomata open to promote atmospheric CO_2 uptake when light is available to power photosynthesis, but this also generates transpiration of water vapour from the inner leaf tissues into the atmosphere. When the light dims, stomata close to prevent inefficient water loss (Vialet-Chabrand et al., 2017). At night, stomata are essentially closed, yet progressive preopening is usually observed before dawn (Caird et al., 2007). Overall, the ability of stomata to track fast changes in irradiance or maintain low transpiration throughout the night enhances plant water use efficiency (Caird et al., 2007; Lawson and Blatt, 2014; Coupel-Ledru et al., 2016; Vialet-Chabrand et al., 2017; Papanatsiou et al., 2019;

Eyland et al., 2021). As water becomes increasingly scarce with climate change, tailoring stomatal dynamics during day and night is a promising strategy to breed crops for drought tolerance. Stomatal movements ultimately result from osmotically-driven changes in turgor pressure of the guard cells, with feedbacks from the epidermal pavement cells and the inner leaf tissues (Lawson and Matthews, 2020; Blatt et al., 2022; Nieves-Cordones et al., 2022). Although the instantaneous effects of light fluctuations on the guard cells are relatively well understood, we lack a mechanistic framework depicting the dynamics of stomatal movements across the diel (24-h) cycle in the context of a whole leaf.

While the diel pattern of stomatal movement is primarily driven by light availability, it also has an endogenous rhythmic component that is controlled by the circadian clock (Hubbard and Webb, 2015). In typical day-night cycles alternating constant light and darkness, stomata start to open several hours before the end of the night, continue to open until the middle of the day, and then engage to close during the afternoon. This endogenous rhythm is under circadian control. For instance, in Arabidopsis, a circadian stomatal rhythm under continuous light is observed in wild-type plants, but is disturbed or even abolished in mutants defective in the circadian clock (Somers et al., 1998; Sothern et al., 2002; Dodd et al., 2004, 2005; Hassidim et al., 2017; Dakhiya and Green, 2019). Despite a strong circadian control, the endogenous stomatal rhythm shows high flexibility upon change in the environmental conditions. In Arabidopsis plants placed in constant irradiance during the day, the timing and amplitude of the diurnal opening differs if plants have been entrained in constant or fluctuating irradiance (Matthews et al., 2018). In *Vicia faba*, nighttime preopening is abolished when plants are shaded on the preceding day, and starts earlier when they are given elevated CO_2 (Easlon and Richards, 2009), suggesting a connection with carbon metabolism. Thus, metabolic cues may counteract, potentiate or interact with the clock to regulate the diel stomatal dynamics.

Starch metabolism and associated sugars could be involved in the diel control of stomatal movements, yet this hypothesis has remained underexplored. While it was early noticed that stomata of the starch-free mutant *pgm* do not preopen at night (Lascève et al., 1997), recent research rather focused on the role of starch and sugar

metabolism in light-induced stomatal opening (Flütsch and Santelia, 2021). In leaf chloroplasts, a fraction of the sugars produced in the day by photosynthesis is accumulated as transitory starch, which is broken down in the following night (Stitt and Zeeman, 2012; Streb and Zeeman, 2012). This diel process of daytime storage and nighttime breakdown, which buffers the diel variations of carbon status against the fluctuations in light availability, occurs mainly in the mesophyll cells. In the guard cells, the turnover of starch is slightly out of phase, with starch synthesis persisting in the early night, and starch degradation accelerating in the early day (Santelia and Lunn, 2017). Rapid guard-cell starch degradation during the first hour of the day is controlled by non-photosynthetic levels of blue light and generates glucose to support stomatal opening (Horrer et al., 2016; Flütsch et al., 2020b). When photosynthesis rises with light, the guard cells import most of their sugars (glucose and sucrose) from the mesophyll; such import further enhances stomatal opening and replenishes the guard-cell starch pool simultaneously (Flütsch et al., 2020b, 2020a). Yet, the general role of sugars in stomatal movements is still debated (Daloso et al., 2016a; Santelia and Lawson, 2016; Daloso et al., 2017; Granot and Kelly, 2019; Lawson and Matthews, 2020; Flütsch and Santelia, 2021). Sugars may trigger stomatal opening by providing the signal, energy or osmotica required for turgor build-up of the guard cells (Outlaw and Manchester, 1979; Poffenroth et al., 1992; Daloso et al., 2015, 2016b; Flütsch et al., 2020a, 2020b). Sugars may also evoke stomatal closure either in the apoplast as osmotica that pull water out of the guard cells (Lu et al., 1997), or in the guard cells through hexokinase-mediated sugar sensing (Kelly et al., 2013, 2019). It has been proposed that sugars induce different effects depending on the carbon status, which covaries with the time of the day, so that sugars promote opening under starvation, like at dawn, but trigger closure upon satiation, like in the afternoon (Flütsch and Santelia, 2021). This working model has remained difficult to test, yet. Moreover, it has not been addressed whether starch metabolism in the mesophyll interferes with this model. While many mutants of the starch metabolism are available with different impacts on sugar content at different times of the diel cycle and in different cell types, we reasoned that obtaining their diel transpiration patterns would provide insight into the spatiotemporal hierarchy of events that connect carbon metabolism and guard cell dynamics throughout the diel cycle.

Here, we developed a phenotyping pipeline to screen the diel transpiration dynamics of a series of Arabidopsis mutants differentially impaired in the starch pathway (Figure 1). We found that severe mutations in starch synthesis (*pgm*, *isa1*) or breakdown (*sex1*, *mex1*) affect the endogenous rhythm of transpiration through a phase shift, which results in delayed stomatal movements throughout the daytime and/or reduced stomatal preopening at night. Strikingly, the endogenous rhythm of one mutant affected in chloroplastic maltose export during starch breakdown (*mex1*) showed a unique sensitivity to low irradiance that was not found in any other starch mutant. Moreover, affecting starch synthesis in the mesophyll but not in the guard cells (*pgi*), blocking starch degradation in the guard cells only (*amy3 bam1*), or impairing starch degradation in both tissues (*bam1 bam3*) did not substantially affect the transpiration dynamics, suggesting cross-tissue metabolic homeostasis may arise depending on the mutations. We concluded that leaf starch metabolism affects the diel dynamics of transpiration indirectly by modulating sugar homeostasis between tissues, most likely through an interaction with the circadian clock – and not through energetic or osmotic effects. Our work sheds light on the regulation of transpiration dynamics, providing new tracks to breed crops for more efficient use of water.

RESULTS

Profiling the diel transpiration dynamics in two extreme starch mutants across environmental conditions highlights an endogenous stomatal rhythm with flexible coordination between day and night

Monitoring transpiration throughout the diel cycle informs us on the dynamics of the processes underlying water loss, but remains a phenotyping bottleneck. We developed PhenoLeaks, a phenotyping pipeline to analyse transpiration dynamics from a temporal series of gravimetrical data. We first adapted a high-throughput phenotyping platform fitted with a mobile scale (Granier et al., 2006) and developed novel scripts so as to monitor the diel kinetics of transpiration on 150 Arabidopsis plants during several days with a 30-min resolution in controlled environmental conditions (Figure 2; Methods). Transpiration of the wild type Col-0 was first measured during ~3 days and nights in

control, growth conditions (400 ppm CO_2, 180 µmol m^{-2} s^{-1} irradiance in the daytime). We observed temporal patterns that could be ascribed to rapid stomatal movements at the day/night transitions and to slower, endogenous stomatal rhythms otherwise (Figure 2C). Stomata opened rapidly when the light switched on, continued to open until the middle of the day and then partly closed until the end of the day. When the light switched off, stomata closed rapidly and, after about 3 h, started to reopen gradually throughout the night. This diel dynamics were consistent with previous data obtained on Arabidopsis using low-throughput, gas exchange analysis (Lascève et al., 1997; Sun et al., 2019) and stomatal aperture measurements (Li et al., 2020). Thus, our phenotyping pipeline reliably captured the broad patterns of transpiration throughout the diel cycle, including endogenous preclosure during the afternoon and preopening at night that produced partial symmetry between the daytime and nighttime patterns.

To get insight into the connection between starch/sugar metabolism and diel stomatal movements, we then examined two extreme mutants that were blocked in either starch synthesis for the starch-free *pgm* or starch breakdown for the starch-excess *sex1*. On the one hand, *pgm* cannot synthesise starch in any cell-type due to ineffective chloroplastic phosphoglucomutase (Caspar et al., 1985; Streb and Zeeman, 2012; Figure 1). On the other hand, *sex1* is defective in the plastidial α-glucan water, dikinase (GWD1) that is responsible for the first step of glucan phosphorylation necessary for starch breakdown (Caspar et al., 1991; Yu et al., 2001; Ritte et al., 2002). In *sex1*, daytime starch synthesis largely exceeds the residual nighttime degradation, resulting in a severe starch-excess phenotype (Streb and Zeeman, 2012; Figure 1A-B), which can be observed in mesophyll cells and also in the guard cells (Azoulay-Shemer et al., 2018; Figure 1C-D). Both *pgm* and *sex1* mutations result in very low starch turnover and generate similar diel variations in the carbon status: during the day, photosynthesis-derived sugars accumulate massively compared to the wild type, but then at night the absence or unusability of starch triggers a rapid depletion of available sugars, resulting in carbon starvation until dawn (Streb and Zeeman, 2012).

Here, the transpiration patterns of the starch mutants differed from that of the wild type, with *pgm* being more affected than *sex1* (Figure 2C-D). To facilitate comparisons of the

transpiration patterns, we extracted the mean transpiration over 24-h (E_{diel}) and over day and night periods (E_{day}, E_{night}), as well as a set of dynamic parameters (Figure 3; Methods). While the mean transpiration rate over each period and the maximal diel amplitude (A_{diel}) were similar in *pgm* as in Col-0 (Supplemental Figure S1A-D), their transpiration patterns were contrasted. In the daytime, the duration of stomatal opening lasted longer in the mutant, which needed about 1.5 h more than Col-0 to reach its maximal transpiration ($t_{day\ max}$, Figure 3D). This delay was not due to a slower rate of light-induced stomatal opening in *pgm*, since the rapid increase in transpiration observed at 30 min after the night-to-day transition ($A_{rapid\ op}$) was similar in *pgm* and Col-0 (Figure 3B). It was rather due to a different endogenous rhythm that appeared to propagate over the rest of the period. This was reflected by a highly significant difference in the rate of endogenous change of transpiration across the day (σ_{day}, Supplemental Figure S1E) associated to a lower afternoon preclosure in *pgm* (Σ_{preclo}, Figure 3F), which compensated for the delay in opening so that the cumulative transpiration due to the endogenous movements (Δ_{day}, Supplemental Figure S1G) was similar – *i.e*. less water loss in the morning but more water loss in the afternoon for *pgm* compared to the wild type. Similar conclusions could be drawn in the nighttime, when the period of slow stomatal closure after the rapid transition was prolonged in *pgm*: the time when transpiration reached its minimum during the night was delayed by about 4 h ($t_{night\ min}$, Figure 3E) in *pgm* compared to Col-0 in spite of similar amplitude of rapid stomatal closure at 30 min after the day-to-night transition ($A_{rapid\ clo}$, Figure 3C). The highly significant difference in the rate of endogenous change of transpiration across the night (σ_{night}, Supplemental Figure S1F) mirrored that observed in the daytime, and virtually no endogenous preopening was observed in *pgm* (Σ_{preop}, Figure 3G), consistent with a previous study (Lascève et al., 1997). In *sex1*, the mean transpiration rates, the diel amplitude, the rapid changes at the transitions, and the daytime pattern were essentially similar as in Col-0 (Figure 3B-D,F, Supplemental Figure S1A-E,G), by contrast with the nighttime endogenous rhythm. Nighttime transpiration after the light-to-dark transition was almost constant in *sex1* (σ_{night} close to zero, Supplemental Figure S1F), making it difficult to estimate $t_{night\ min}$ with good precision for this mutant (high variance of this parameter, Figure 3E). Nevertheless, nighttime preopening was clearly reduced in *sex1*,

resembling *pgm* (Figure 3G). Thus, while severe mutants in starch synthesis (*pgm*) and breakdown (*sex1*) showed broadly similar leaf carbon status in the daytime (over-satiation) and the nighttime (starvation), their transpiration phenotype appeared to be shared only at night. This suggests that the daytime carbon status is not equivalent in both mutants, or that the transpiration dynamics is not directly connected to leaf carbon status.

To further explore the effect of varying carbon status on diel transpiration, we then subjected the same plants to one day of elevated CO_2, followed by one day of low irradiance and two days of recovery (Figure 2C-D). For the wild type, doubling the atmospheric CO_2 (800 ppm) resulted in a 25% enhancement of daytime starch accumulation (Figure 2B). Concurrently, mean daytime transpiration decreased by 15% (Supplemental Figure S1C) with a similar reduction in $A_{rapid\ op}$ (consistent with stomatal response to elevated CO_2, Zhang et al., 2018; Figure 3B), while the daytime parameters describing the endogenous dynamics varied only marginally (Figure 3D,F, Supplemental Figure S1E,G). At night, CO_2 was returned to 400 ppm. The remaining starch at the end of the night almost tripled (Figure 2B). Nighttime transpiration was barely affected (Supplemental Figure S1D), except in the early night when transpiration appeared more stable than in the control condition (as reflected by the higher variance of $t_{night\ min}$), but the associated reduction in Σ_{preop} was hardly significant (Figure 3E,G). Thus, increasing starch turnover through elevated CO_2 was not associated with remarkable changes in the endogenous stomatal rhythm. In the following day, the plants were subjected to low irradiance (50 µmol m^{-2} s^{-1}), which dramatically reduced daytime starch synthesis (Figure 2B). Compared to the control environment, daytime transpiration decreased by 25% (Supplemental Figure S1C). This resulted from a reduction in $A_{rapid\ op}$ (consistent with stomatal response to irradiance, Shimazaki et al., 2007; Figure 3B), but also from significant changes in the daytime endogenous dynamics, with $t_{day\ max}$ being advanced by almost 3 h (Figure 3D) and Δ_{day} being highly significantly reduced (Supplemental Figure S1G). This resulted in a lower transpiration rate at the end of the daytime and consequently, transpiration in the following night also decreased (Supplemental Figure S1D), with a slight reduction in Σ_{preop} (Figure 3G). Thus, reducing starch turnover through low irradiance produced different effects than the *pgm* or *sex1* mutations,

depending on the parameter. Finally, two days of recovery in control environment showed that diel transpiration retrieved its original dynamics, with a global trend of transpiration attenuation as the rosette developed (Figure 2C, Supplemental Figure S1A-D). The dynamics were essentially similar between the two days, yet Σ_{preop} and σ_{night} were significantly lower in the last night (Figure 1I, Supplemental Figure S1G). Overall, the mean transpiration rates, diel and transitional amplitudes were much more affected by the daytime environment than by the *pgm* and *sex1* mutations, as indicated by the respective ANOVA effect sizes (η^2_g, Figure 3B-C, Supplemental Figure S1A-D). By contrast, for the dynamic parameters describing the endogenous rhythm, the genotype and the environment were equally important in the daytime, and the genotype dominated at night (Figure 3D-G, Supplemental Figure S1E-H). While significant genotype by environment interaction could be detected on some parameters, the effect size of the interaction remained always lower than the size of the main effect(s), indicating that *pgm* and *sex1* responded to the environment essentially as the wild type. This observation further supports the idea that changes in starch turnover are not required to support the changes in transpiration dynamics induced by the environments.

We drew two conclusions from these results. First, there is a 'flexible coordination' between day and night transpiration dynamics, so that changes in the daytime patterns broadly echo at night, yet with some asymmetry. For instance, genetic and environmental perturbations may affect daytime patterns similarly as nighttime patterns (compare Figure 3B *vs*. 3C, 3D *vs*. 3E, 3F *vs*. 3G, Supplemental Figure S1C *vs*. S1D, S1E *vs*. S1F) but not systematically (e.g. *sex1* in Figure 3F *vs*. 3G, Supplemental Figure S1E *vs*. S1F). Second, disturbing starch metabolism may coincide with important changes in the endogenous rhythm of transpiration both day and night, but starch turnover *per se* is likely not instrumental in these changes.

Modelling the diel dynamics of transpiration reveals that blocking starch metabolism induces a phase shift in the endogenous stomatal rhythm

The flexible coordination between day and night patterns of transpiration, and the circadian nature of the endogenous stomatal rhythm (Hubbard and Webb, 2015),

prompted us to build an overarching framework that could capture daytime and nighttime traits through a common set of parameters. This was achieved by designing a sinusoidal model (Figure 4; Methods), where diel transpiration shows step changes at the day/night transitions, and oscillates throughout the whole day and night cycle according to a periodic, sinusoidal signal. The temporal response of stomata to a rapid change in light intensity, which predominates at the day/night transitions, follows an exponential kinetics with a time constant (*i.e*. the duration for reaching 63% of the full response) typically of about 20 min for opening and 5 min for closure in Arabidopsis (Matthews et al., 2018). Such temporal variations were too rapid to be captured with good precision in our experiments due to the 30-min resolution, so we used a square wave at the day/night transitions (equivalent to a time constant of 0 min) in the model. Hence, stomatal opening and closure at the day/night transitions were considered as broadly symmetrical, which was a reasonable assumption given that similar values were obtained for $A_{rapid\ op}$ and $A_{rapid\ clo}$ in steady conditions (Figure 3B-C). For the rest of the diel cycle, we implemented a periodic signal composed of a fundamental sine wave (period fixed to 24 h) and its second harmonic (period fixed to 12 h), which allowed for asymmetry between daytime and nighttime patterns.

The model had only six parameters that were shared between day and night and easily interpretable: the mean transpiration rate over a 24 h period (E_{mean}, mmol m^{-2} s^{-1}); the semi-amplitude of the square wave (A_{SQW}, mmol m^{-2} s^{-1}), which accounts for stomatal opening and closure at the day/night transitions; the semi-amplitudes of the sine waves (A_1 for the fundamental wave and A_2 for the second harmonic, mmol m^{-2} s^{-1}), which set the magnitude of the endogenous rhythm; and the phases of the sine waves (φ_1 and φ_2, h), which set the timing of the endogenous rhythm. A major strength of this model is that it could be fitted using linear regression (once appropriately transformed), making the parameter estimation robust (Methods). For the control days in steady environmental conditions and for each plant, we fitted one set of parameters over the entire period of 2.75 d (example in Figure 4A). For the other environmental conditions, we repeated the fit every 24 h considering one day and its following night – implicitly assuming that the endogenous rhythm would respond rapidly to the change. We also extracted from the fitted curves the same parameters as for the measured data (Figure 4B). Across the

whole dataset (17 genotypes $\times$ 5 environments), the adjusted R^2 averaged 0.99 and was never lower than 0.88, indicating excellent agreement between the model and the data.

Analysing the fitted parameters highlighted the architecture of the diel dynamics, and revealed distinct phase shifts depending on the starch mutants (Figure 4C-H). In control conditions and in all genotypes, the magnitude of the rapid responses at the day/night transitions (A_{SQW}) was similar as the magnitude of the endogenous rhythm (A_1+A_2), with the fundamental wave largely dominating over the second harmonic (A_1 being three to four times higher than A_2). Accordingly, the fundamental sine peaked around the middle of the daytime, about 1 h before midday for Col-0 in control conditions ($\varphi_1 = +1.28 \pm 0.23$ h, meaning that the peak is at $24 / 4 - 1.28 = 4.72$ h after the light switches on). The second harmonic peaked around midday too, and also around midnight (for Col-0, $\varphi_2 = -2.72 \pm 0.18$ h, meaning that the peaks are at $12 / 4 + 2.72 = 5.72$ h after the light switches on and off). Consequently, the variations of the second harmonic were relatively well synced with that of the fundamental sine during the day (thereby enhancing the endogenous transpiration rhythm), but had an opposite behaviour at night (thereby attenuating the endogenous rhythm). Manipulating the environment reduced the amplitudes, with A_{SQW} being more sensitive to elevated CO_2 and A_1 to low irradiance, while A_2 remained mostly unaffected. Comparatively, genotypes had much less influence on the amplitudes, excepted *pgm* that often showed higher A_1. By contrast, the genotypes had strong effects over the phases. We uncovered a marked phase shift on φ_1 with more than 2 h delay in *pgm*, which was conserved across the environments. We observed a smaller phase delay of 45 min for φ_2. In *sex1*, φ_1 was similar as in Col-0, while φ_2 was 45 min ahead. On the other hand, there was no significant effect of elevated CO_2 on the phases, while low irradiance induced a phase lead of almost 1.5 h for both φ_1 and φ_2 in all genotypes. Thus, shifting the phase of the fundamental sine resulted in a global lead (low light) or delay (*pgm*) in the endogenous rhythm, while independent phase modulation of the second harmonics resulted in different effects on the afternoon preclosure (*pgm* only) and nighttime preopening (*pgm* and *sex1*), which were recapitulated by the model (compare Figures 2H-I and 4I-J).

To get a hierarchical view of the components underlying the diel dynamics, we then generated a heatmap covering the whole dataset (Figure 5). The extracted parameters from the data and from the fitted curves were closely related, supporting the quality of the model. A clustering analysis revealed that the parameters related to the diel and transitional amplitudes grouped together, and were separated from the parameters describing the endogenous rhythm. The parameter A1 clustered together with Δ_{day} (measured and fitted) while A_2 was more isolated, confirming the prevalence of the fundamental wave. Interestingly, φ_1 was closely related to σ_{night}, Σ_{preop} and to a lesser extent Δ_{night}, highlighting a strong influence of this phase over nighttime stomatal behaviour. On the other hand, φ_2 clustered together with Σ_{preclo}. The individuals were primarily clustered according to the environmental conditions, due to a strong effect on the baseline transpiration and amplitudes; however, *pgm* disrupted the main ranking, together with another mutant that will be presented later (*mex1*), due to strongly altered endogenous rhythm.

Comparing mutants of starch metabolism pinpoints a key role for maltose export in controlling the endogenous rhythm of transpiration

To get deeper insight into the connection between diel transpiration dynamics and starch metabolism, we then scrutinized the behaviour of the individual mutants, starting by the biosynthesis pathway downstream of PGM. We first examined two mutants with mild reduction in starch synthesis, which both exhibited differences in transpiration dynamics compared to the wild type, yet not on the same parameters (Figure 6, Supplemental Figure S2). On the one hand, *isa1* is impaired in the debranching enzyme isoamylase 1, which contributes to the structure of starch; it accumulates phytoglycogen rather than only starch and shows premature exhaustion of its reserves during the night (Delatte et al., 2005; Wattebled et al., 2005; Figure 1). Here, *isa1* had a transpiration phenotype resembling that of *pgm*, with disturbed rates of change of the endogenous rhythm (σ_{day} and σ_{night}, Supplemental Figure S2G,K) and reduced nighttime preopening (Σ_{preop}, Figure 6J) that coincided with a φ_1 delay of 1.3 h (Figure 6G). On the other hand, *ss4* is affected in starch synthase 4, which is required for the initiation of starch granules; it has

reduced starch synthesis and, contrary to *isa1*, incomplete nighttime breakdown (Roldán et al., 2007; Crumpton-Taylor et al., 2013; Lu et al., 2018; Figure 1). In our assay, the endogenous transpiration rhythm of *ss4* had unaltered phases but showed lower magnitudes A_1 and A_2 (Figure 6E-H), which reduced A_{diel} (Supplemental Figure S2B). These results confirmed that disturbing starch metabolism may trigger different changes in the diel dynamics of transpiration, but that starch turnover does not simply drive the endogenous stomatal rhythm.

We next examined the influence of starch degradation downstream of SEX1 and uncovered a key role for chloroplastic maltose transport in the diel transpiration dynamics (Figure 7, Supplemental Figure S3). Maltose is the main product of nighttime starch breakdown in the mesophyll chloroplasts; it is generated by β-amylases and then exported to the cytosol by the MALTOSE EXCESS 1 (MEX1) chloroplastic transporter (Niittylä et al., 2004; Weise et al., 2004, 2005; Figure 1A). The *mex1* mutant over-accumulates maltose in the chloroplast and is impaired in starch breakdown (Niittylä et al., 2004; Lu et al., 2006). The function of MEX1 in starch metabolism of the guard cells is not documented. Intriguingly, we noticed that the guard cells of *mex1* appeared essentially devoid of starch, contrary to the rest of the leaf that had starch in excess (Figure 1B-D). This spatial pattern was unique across all the mutants we monitored. In control conditions, the endogenous transpiration dynamics of *mex1* showed disorders like in *pgm* and *isa1*, with altered σ_{day} and σ_{night} (Supplemental Figure S3G,K) and reduced nighttime preopening (Figure 7K) that were subtended by a φ_1 delay of 1.9 h. Moreover, *mex1* was exquisitely sensitive to changing environmental conditions, especially low irradiance. The baseline transpiration E_{mean} was much more markedly affected by elevated CO_2 and low irradiance in *mex1* compared to the wild type, yielding highly significant differences between both genotypes in these non-control conditions (Figure 7D). Both E_{day} and E_{night} were affected (Supplemental Figure S3E,I). After the day at elevated CO_2, transpiration continuously dropped in the following night (Figure 7A). Then, under low irradiance, the rapid opening at the night-to-day transition $A_{rapid\ op}$ was similar as in Col-0 (Supplemental Figure S3C), but the amplitude of the endogenous rhythm A_1 was significantly reduced (Figure 7F). During the following night, transpiration steadily flowed at a low level (Figure 7A). These aberrant stomatal responses of *mex1*

might arise from a loss of chloroplast integrity in this mutant, which develops chlorotic leaves with chloroplasts showing autophagy-like degradation (Stettler et al., 2009). For instance, chloroplast degradation could disrupt the production of regulatory signals from the mesophyll (Lawson and Matthews, 2020), or prevent turgor generation within the guard cells (Azoulay-Shemer et al., 2015). However, disturbed environmental conditions were unlikely to produce irreversible chloroplastic damages: upon return to the original growth conditions, the diel dynamics remarkably recovered the same baseline as the wild type, which was mediated by a strong increase in the amplitude of the endogenous rhythm (A_1 and A_2), but not in $A_{rapid\ op}$, in the first day of recovery (Figure 7D-G, Supplemental Figure S3A,C). Accordingly, this behaviour translated into an upsurge in σ_{day} (Supplemental Figure S3G). Across our experiment, no mutant other than *mex1* showed such marked sensitivity to environmental conditions, pinpointing the importance of the transporter therein.

Analysis of two other mutants in this pathway further supported the view that maltose export influences the diel dynamics of transpiration (Figure 7, Supplemental Figure S3). Next to maltose, glucose is produced by the chloroplastic disproportionating enzyme 1 (DPE1) during starch breakdown (Critchley et al., 2001), and is further exported to the cytosol by the glucose transporter pGlcT (Cho et al., 2011; Figure 1A). The glucose route is parallel to the maltose route and is thought to be minor (Streb and Zeeman, 2012). Here, blocking the glucose pathway in *dpe1* affected starch turnover similarly as in *mex1* (Figure 1B), but resulted in contrasting transpiration dynamics: the diel pattern of *dpe1* (Figure 7C) resembled more that of the wild type, yet φ_1 was advanced by 1 h and $t_{night\ min}$ by 2.4 h, and A_1 was slightly reduced (Figure 7F,H, Supplemental Figure S3J). Contrary to *mex1*, no major difference was observed upon changing the environmental conditions. We then looked at *dpe2*, a mutant affected in the cytosolic disproportionating enzyme 2 that uses the maltose exported by MEX1 to release glucose (Streb and Zeeman, 2012; Figure 1A). The *dpe2* mutant has a starch-excess phenotype (Figure 1B), and accumulates extremely high levels of maltose in the cytosol throughout the diel cycle (Lu et al., 2006; Chia et al., 2004; Lu and Sharkey, 2004; Weise et al., 2005). We observed transpiration phenotypes in *dpe2* (Figure 7C) that were opposite to that in *mex1*, with enhanced nighttime preopening as well as lower

$t_{night\ min}$ and higher σ_{night}, which were concomitant with a φ_1 lead of 1.2 h compared to Col-0 in control conditions (Figure 7H,K, Supplemental Figure S3J,K). Switching to elevated CO_2 or low irradiance triggered similar changes in *dpe2* as in the wild type, but return to the original conditions induced an upsurge in stomatal preopening (Figure 7C,K, Supplemental Figure S3K). These results supported a role for maltose export in promoting nighttime stomatal preopening by advancing the phase of the endogenous rhythm.

We noted, however, that feeding leaves with high concentration of exogenous maltose (1 mM) through the transpiration stream had no obvious short-term effect on stomatal dynamics, either in the dark, in the light, or during a dark-to-light transition (Supplemental Figure S4). Moreover, it is not known if MEX1 functions as a maltose exporter in the guard cell chloroplasts, and if starch breakdown in the guard cells actually produces maltose to be exported (Santelia and Lunn, 2017). Hence, it was unclear whether the observed phenotypes were due to guard-cell-autonomous metabolic dysfunctions, or remote effects from the mesophyll metabolism.

Neither guard-cell-autonomous nor bulk-leaf starch turnover may directly sustain diel stomatal dynamics

We next analysed genotypes that are differentially affected in guard-cell *vs*. mesophyll-cell starch metabolism (Figure 8, Supplemental Figures S5, S6, S7). We focused on the *pgi* mutant, which is defective in the plastidial phosphoglucose isomerase that produces Glc6P from Fru6P upstream of PGM (Yu et al., 2000; Figure 1A). While starch synthesis is largely impaired in *pgi*, some cell types can bypass the PGI step by importing Glc6P directly from the cytosol (Overlach et al., 1993; Niewiadomski et al., 2005; Flütsch et al., 2022; Figure 1A). Accordingly, *pgi* is essentially starch-deficient in the mesophyll cells, but retains starch synthesis in several cell types including the guard cells (Tsai et al., 2009; Kunz et al., 2010; Azoulay-Shemer et al., 2016; Figure 1D), resulting in a reduced daytime starch accumulation when measured at the bulk-leaf level (Figure 1B-C). Here, no difference in the transpiration dynamics was found between *pgi* and the wild-type, except a slight shift in the baseline (Figure 8A,D-K, Supplemental Figure S5). Does this

result mean that guard cells hold the pool of starch that supports their own diel dynamics?

We tested this cell-autonomous hypothesis, but could not find evidence to support it. Starch degradation in the guard cells is achieved through the guard-cell specific and synergistic action of the isoforms α-amylase AMY3 and β-amylase BAM1 (Horrer et al., 2016; Flütsch et al., 2020b; Figure 1A). The double mutant *amy3 bam1* is severely impaired in starch degradation in the guard cells but has intact starch turnover in the bulk leaf (Figure 1B-D). Here, the diel dynamics of transpiration of *amy3 bam1* were virtually indistinguishable from that of Col-0 (Figure 8B), just like the single mutants (Supplemental Figure S6A-B). No significant difference could be detected in the measured or fitted parameters between Col-0 and *amy3 bam1* in control conditions (Figure 8D-K, Supplemental Figure S5). Across all environments and all parameters, we only observed an increase in $t_{night\ min}$ after low irradiance and a reduction in Σ_{preclo} on the first day of recovery, but the effect size and significance remained low. This result demonstrated that guard cell-autonomous starch breakdown is not required to achieve proper diel stomatal movements.

Alternatively, it might be plausible that the pool of starch from the mesophyll can substitute for that from the guard cells, and vice versa. We therefore looked at two other mutants affected in the family of β-amylases. BAM3 is normally the main isoform involved in mesophyll starch degradation but in its absence, BAM1 partly compensates its function (Fulton et al., 2008). Accordingly, the *bam3* single mutant has an intermediate starch-excess phenotype in the mesophyll only, while the *bam1 bam3* double mutant has a severe starch-excess phenotype in the mesophyll and in the guard cells (Fulton et al., 2008; Horrer et al., 2016; Figure 1B-D). Thus, under the hypothesis of pool substitution between cell types, we would expect *bam3* to have similar transpiration dynamics as Col-0, and *bam1 bam3* to resemble *mex1* or *sex1*. Here, in control conditions, *bam3* showed reduced E_{mean}, A_1, A_2 and a φ_1 lead of 1 h compared to Col-0 (Supplemental Figure S6C-K), while *bam1 bam3* behave similarly as the wild type (Figure 8C-K). Changing the environment affected these differences only marginally (Figure 8C-K, Supplemental Figures S5, S6 C-K, S7). Hence, no direct connexion could

be done between diel transpiration dynamics and starch turnover, either in the guard cells or in the rest of the leaf, suggesting more complex spatiotemporal effects. It should be noted, though, that functional interactions within the BAM family generate atypical patterns of maltose production in the *bam* mutants. For instance, at the start of the day, leaf maltose content is actually higher in *bam3* than in Col-0, while that in *bam1 bam3* is similar as in the wild type (David et al., 2022). This may be important if maltose, or a sugar derivative, shifts the endogenous stomatal rhythm by acting at a specific time of the diel cycle.

Beyond sugars, an alternative candidate could be malate, which is thought to coordinate mesophyll photosynthesis and stomatal behaviour (Araújo et al., 2011; Daloso et al., 2017). However, two independent mutants impaired in ABCB14, a guard cell malate importer (Lee et al., 2008) with normal starch turnover (Supplemental Figure S8), showed diel dynamics of transpiration that were virtually indistinguishable from that of the wild type (Figure 9, Supplemental Figure S9).

DISCUSSION

The PhenoLeaks pipeline for monitoring the diel dynamics of transpiration highlights an endogenous stomatal rhythm that is shared between day and night

Tailoring stomatal dynamics emerges as a realistic strategy for improving water use efficiency (Papanatsiou et al., 2019), but progress has been hindered by the lack of accessible phenotyping systems to monitor the genotypic variability for temporal patterns of transpiration. Here, we developed the PhenoLeaks pipeline to extend the capabilities of an existing phenotyping system initially designed to control soil water content by gravimetry (Granier et al., 2006), allowing us to monitor the diel transpiration dynamics on 150 pots with a 30-min resolution. We obtained similar dynamics as in previous Arabidopsis studies that used whole-plant gas exchange systems (Lascève et al., 1997; Sun et al., 2019), but also single leaf porometry (Matthews et al., 2018; Li et al., 2020) and direct measurements of stomatal aperture (Hassidim et al., 2017; Li et al., 2020). This indicates that the diel dynamics in transpiration are essentially driven by

stomatal movements, while other factors potentially influencing the patterns of transpiration and also showing diel variations (Apelt et al., 2015), such as growth (that affects the leaf area by which transpiration is normalized) and hyponasty (that may affect the boundary layer conductance), are of secondary importance. Our calculations of transpiration assume constant growth rate of the transpiring area, not only because leaf expansion is not trivial to monitor at high temporal resolution, but also because we do not know how closely the acquisition of stomatal function paces tissue morphogenesis. Nonetheless, considering the available patterns of diel areal growth in Col-0 and *pgm* (Apelt et al., 2015) would make their diel dynamics to get closer together at night (growth of *pgm* is almost null after 4 h, but decreases only slowly in Col-0), but to be still more delayed during the day (growth in Col-0 is temporarily dampened during the two first hours of the day, while that of *pgm* is boosted). Thus, delayed transpiration in *pgm* arises from stomatal behaviour. Moreover, the transpiration dynamics were also consistent with the expected responses of stomata to elevated CO_2 (Zhang et al., 2018) and low irradiance (Shimazaki et al., 2007). Incidentally, there was a decreasing trend of transpiration rate as the experiment progressed, consistent with the idea that the leaf surface of Arabidopsis globally waterproofs as the plant ages. On the one hand, each leaf shows decreasing transpiration as it develops, which results from a gradual priming of stomatal function and a decrease in cuticular permeability (Pantin et al., 2013b; Kane et al., 2020; Hõrak et al., 2021). On the other hand, the proportion of young leaves (with higher transpiration) decreases as the rosette grows. Incomplete waterproofing through stomatal or cuticular leakiness are also both likely to explain why the baseline of nighttime transpiration is so high in Arabidopsis (more than 50% of daytime transpiration), at least when grown indoors in non-stressful conditions. Overall, beyond the baseline, our setup was amenable for tracking diel stomatal rhythms of various genotypes over several days in contrasting environments. The PhenoLeaks pipeline can readily be applied to any time-series of weight data obtained on any species.

PhenoLeaks also enabled us to provide a quantitative framework that accounts for the diel dynamics of transpiration, overarching daytime and nighttime stomatal movements and thereby hinting at the circadian clock. A previous model published by Matthews et al. (2018) accounted for both the rapid stomatal responses to light fluctuations and the

endogenous daytime rhythm, but nighttime transpiration was not considered. In their model, the endogenous daytime rhythm was described as an exponential decrease that superimposed to a Gaussian, bell-shape signal, involving five parameters to be estimated by non-linear procedures. Here, we propose a simple sinusoidal model that can be readily transformed and fitted through linear regression, with only four parameters (amplitudes A_1 and A_2, phases φ_1 and φ_2) to describe the endogenous rhythm of transpiration both day and night. It is not only robust and parsimonious, but also offers guidance for the physiology behind the parameters. Decomposition of a rhythmic signal into a series of periods, amplitudes and phases is a classical approach in the field of the circadian clock (Plautz et al., 1997). Studies in other organisms have revealed that the expression of many genes oscillates with a 24-h period but also with a 12-h period (Hughes et al., 2009), and the idea that the circadian clock may generate harmonic oscillations has gained theoretical and experimental support (Westermark and Herzel, 2013; Martins et al., 2016). In Arabidopsis like in many plants, there is strong diel rhythmicity for starch and sugar metabolism, and it is partly under circadian control (Bläsing et al., 2005; Lu et al., 2005). Moreover, the endogenous stomatal rhythm itself is under circadian control (Hubbard and Webb, 2015). Thus, that the rhythmic patterns of stomatal movements show harmonic oscillations makes biological sense. But does starch metabolism affect stomatal rhythm by interfering with the clock, or by introducing independent effects?

The tempo of starch metabolism and its sugar by-products does not coincide with the endogenous rhythm of transpiration, either in the daytime or in the nighttime

While we provide evidence for a strong link between starch metabolism and the timing of diel stomatal movements, starch turnover could not be defined as a reliable integrator linking both processes. Disturbing starch metabolism through genetic or environmental manipulations affected the endogenous rhythm of transpiration, yet not systematically. Three mutants with severely altered starch turnover showed shifted transpiration dynamics during the day as well as impaired stomatal preopening at night that coincided

with a delay in the fundamental phase φ_1.These mutants included *pgm* that cannot synthesize starch (Caspar et al., 1985), *isa1* that mostly produces phytoglycogen instead of starch (Delatte et al., 2005; Wattebled et al., 2005; Streb et al., 2008), and *mex1* that cannot transfer maltose outside the chloroplast during nighttime starch breakdown (Niittylä et al., 2004). Moreover, *sex1* that cannot initiate starch breakdown also showed reduced nighttime preopening, yet driven by an advanced φ_2. At first glance, these behaviours supported a causal link between starch turnover and diel stomatal movements. However, other observations contradicted this idea, and the diel rhythm of transpiration could not be consistently associated with starch turnover, either in the guard cells or in the rest of the leaf. For example, abolishing starch breakdown in the guard cells of *amy3 bam1* or reducing starch synthesis in the mesophyll of *pgi* did not markedly affect the diel pattern of transpiration. Affecting starch degradation of both cell types in *bam1 bam3* did not provoke further transpiration phenotype. Moreover, other mutations (*dpe1*, *dpe2*, *bam3*) as well as low irradiance led to reduced starch turnover and yet advanced φ_1. Thus, further interpretation of the transpiration dynamics required examining traits related to starch metabolism but not starch turnover *per se*.

Soluble sugars that circulate in the plant day and night provided credible rhythmic candidates linking starch metabolism and stomatal movements, and yet this hypothesis could not be easily reconciled with our data. Sugars have been associated with stomatal opening or closure, possibly depending on the time of the day, the sugar species, its concentration or localization (Granot and Kelly, 2019; Flütsch and Santelia, 2021). A working model is that sugars promote stomatal opening upon starvation, and closure upon satiation, but it has remained difficult to test because the available data for sugar concentration lack spatiotemporal resolution, and because there is often covariation between carbon status and time of the day. Here, there was no robust link across genotypes between the transpiration patterns and the published patterns of major sugars (sucrose, glucose, fructose). Let us focus on the daytime. At dawn, mesophyll photosynthesis yields glucose and sucrose which promote light-induced stomatal opening (Flütsch et al., 2020a, 2020b). It is conceivable that these photosynthesis-derived sugars add to the pool of apoplastic sugars remaining from starch degradation of the previous night. Thus, in starch mutants, we might expect that a lack of starch-

derived apoplastic sugars at the night-to-day transition results in slower stomatal opening. However, should this effect exist, it would be very transient (< 30 min) or of low magnitude. First, there was no significant difference in $A_{rapid\ op}$ between the mutants and the wild-type, confirming previous findings on *pgm* (Lascève et al., 1997). Comparatively, stomata of the double mutant *stp1 stp4*, which lacks key glucose importers in the guard cells, have barely started to open after 2-h illumination (Flütsch et al., 2020a). Second, shortly after the onset of illumination, massive amounts of soluble sugars are found in the leaves of starch mutants such as *pgm* (Caspar et al., 1985) or *sex1* (Caspar et al., 1991). For instance, 2 h after dawn, the content in sucrose and reducing sugars is already more than two times higher in *pgm* than in wild-type leaves (Gibon et al., 2004b; Pal et al., 2013), while transpiration of the mutant is still lagging behind. It is therefore unlikely that the lack of exported sugars impedes stomatal opening during several hours in the starch mutants. Alternatively, one could argue that the excess of sugars in starch mutants hampers stomatal opening in the morning as observed in *pgm* and *mex1*. Consistent with this hypothesis, the overflow of photosynthetic sugars imported by the guard cells has been proposed to close stomata through hexokinase sensing (Kelly et al., 2013; Lugassi et al., 2015). Nevertheless, the *pgi* mutant also accumulates high levels of sugars shortly after dawn (Kunz et al., 2010) and yet shows similar daytime dynamics of transpiration as in the wild type. Moreover, in the afternoon, sugar content remains higher in *pgm* than in Col-0, and yet stomata of the mutant start closing later. Thus, there was no univocal relationship across the genotypes between the content in major soluble sugars and daytime stomatal movements.

We have also addressed the possibility that maltose, the main outcome of starch breakdown, acts as a signal for nighttime stomatal preopening, but we failed in establishing a causal relationship. Since the first observation one century ago that stomata preopen throughout the night (Loftfield, 1921), this behaviour has been reported in many species (Schwabe, 1952; Caird et al., 2007). Based on gas exchange experiments in *Vicia faba*, it was suggested that a by-product of starch metabolism could be the molecular link between daytime photosynthesis and stomatal preopening in the following night (Easlon and Richards, 2009). While *amy3 bam1* cannot break starch down in the guard cells and yet had no transpiration phenotype, it remained plausible

that a fraction of sugars produced by nighttime starch degradation in the mesophyll gradually diffuses into the apoplast, reaches the guard cells and sustains stomatal preopening as the night progresses. Maltose is the major route for nighttime starch breakdown. It remains trapped in the chloroplasts of *mex1* (Niittylä et al., 2004), which showed strong reduction in nighttime preopening. By contrast, *dpe2*, known for its extremely high cytosolic maltose content (Lu et al., 2006), showed the highest nighttime preopening. Moreover, *pgm* and *isa1* have altered maltose production (Niittylä et al., 2004; Delatte et al., 2005) and reduced nighttime preopening, while *dpe1* and *ss4* have almost normal maltose content (Critchley et al., 2001; Roldán et al., 2007) and almost normal nighttime preopening. Thus, mobile maltose could promote gradual preopening at night. Consistent with this premise, maltose transport is detected in phloem exudates of Arabidopsis leaves (Lu et al., 2006), while exogenous maltose added on epidermal peels is metabolized by guard cells (Dittrich and Raschke, 1977) and gently enhances stomatal opening (Dittrich and Mayer, 1978). However, feeding leaves with exogenous maltose through the transpiration stream did not elicit stomatal opening. Moreover, both *pgi* and *bam1 bam3*, which have impaired maltose production (Weise et al., 2004; Fulton et al., 2008; David et al., 2022), showed intact nighttime preopening. Thus, we could not confidently conclude that maltose is a mobile signal that promotes nighttime stomatal preopening. Furthermore, in Arabidopsis under short-day conditions, maltose production decreases compared to long-day conditions (Lu et al., 2005) but stomatal preopening is enhanced, accelerating at the end of the long night (Leymarie et al., 1998; Lebaudy et al., 2008). On the other hand, nighttime preopening is altered in mutants with impaired circadian clock (Dodd et al., 2005; Hassidim et al., 2017; Dakhiya and Green, 2019). We therefore favour the view that stomatal preopening at night is integral of a diel endogenous rhythm that is controlled by the circadian clock, which in turn interacts with photoperiodism and carbon metabolism.

Starch and sugars plausibly affect the endogenous rhythm of transpiration through interplay with the circadian clock

We propose that starch and sugars affect the timing of the endogenous rhythm of transpiration through an interplay with the clock, not through an independent, instantaneous role. Starch and sugar metabolism interacts with the clock in various ways. For instance, nighttime starch degradation is under circadian control (Graf et al., 2010). Conversely, in the dark, sucrose regulates the circadian clock through stabilization of its *GIGANTEA* component (Dalchau et al., 2011; Haydon et al., 2017). Moreover, in the early morning the clock is entrained by photosynthesis-derived sugars through the *PSEUDO-RESPONSE REGULATOR 7* component (Haydon et al., 2013). This is mediated by the transcription factor BASIC LEUCINE ZIPPER 63, itself regulated by the sugar-sensing kinase SnRK1 (Frank et al., 2018). Interestingly, sugars advance the phase of the clock in the morning, but delay it at night (Haydon et al., 2013), which would feedback on starch degradation rate and maintain carbon homeostasis throughout the diel cycle (Seki et al., 2017). Thus, abnormal sugar fluctuations triggered by mutations in the starch pathway (or by changes in the environment) may disturb the phase of the clock and the endogenous stomatal rhythm, with different effects depending on the timing and magnitude of the metabolic perturbations. Subtle differences in the spatiotemporal patterns of sugar content, such as for *pgm vs*. *pgi*, or *sex1 vs*. *bam1 bam3*, may then generate different phase shifts within the guard cells, underlying the inconsistent association between bulk-leaf starch turnover and stomatal movements.

How could an interplay between sugar metabolism and the clock ultimately modify stomatal movements? It is likely that sugars coming from the mesophyll add to the sugar pool of the guard cells, where they may adjust the local clock (that is tissue-specific; Endo, 2016), and finally ion transport. An attractive candidate at the crossroads of sugar metabolism, circadian clock and ion transport in the guard cells is the florigen FT (FLOWERING LOCUS T), as well as its paralog TSF (TWIN SISTER OF FT). FT and TSF are normally involved in the photoperiodic control of flowering, and their induction requires trehalose-6-phosphate, a metabolic intermediate considered as a signal of carbon satiation (Wahl et al., 2013). In the guard cells, FT and TSF are controlled by several proteins involved in the circadian clock and photoperiodism (EARLY FLOWERING 3, GIGANTEA, CONSTANS) and gate the signalling pathway responsible

for blue-light-induced stomatal opening (Kinoshita et al., 2011; Ando et al., 2013). Moreover, the *ft* mutant in continuous light has barely open stomata that are devoid of circadian rhythm (Kinoshita et al., 2011). The presence of FT, governed by the clock, would then permit light-activation of the plasma membrane H^+-ATPase (Hubbard and Webb, 2011; Kinoshita et al., 2011). The activity of H^+-ATPase energizes solute transport and impacts transpiration (Merlot et al., 2007; Blatt et al., 2014). H^+-ATPase activity in the guard cells enhances the baseline of stomatal aperture in the daytime and the nighttime (Costa et al., 2015) and is a major limiting factor for light-induced stomatal opening (Wang et al., 2014), for instance by stimulating the activity of inward K^+ channels, which are key effectors in stomatal opening (Jezek and Blatt, 2017). Interestingly, the *kincless* mutant, which is impaired in inward K^+ current, displays defects in transpiration dynamics, with slowed daytime opening, impeded nighttime preopening, and impaired circadian rhythm (Lebaudy et al., 2008). Thus, in starch mutants such as *pgm*, *isa1*, *sex1* or *mex1*, strong metabolic disorders – including in the mesophyll – that eventually upset sugar availability within the guard cells may locally translate into a phase shift in the circadian clock, which would then delay FT production, H^+-ATPase activity, K^+ import, turgor build-up and stomatal (pre)opening. Such working model contrasts with the prevailing model whereby sugars from mesophyll-photosynthesis and from guard-cell starch degradation affect light-induced stomatal opening by supporting a metabolic activity that yields ATP in the guard cells, thereby empowering ion transport (Daloso et al., 2017; Flütsch and Santelia, 2021). While our work does not dismiss the importance of this model upon light fluctuations like at the night-to-day transition, it suggests that starch and sugar metabolism exerts control over the diel rhythm of stomatal movements through distinct spatiotemporal effects, involving a phase shift in the guard cells tempo.

Spatiotemporal regulation of guard cell metabolism and stomatal movements

Additional mechanisms linked to carbon metabolism – and possibly to the clock – may also contribute to shift the endogenous rhythm of transpiration in the starch mutants. First, there could be a temporal mismatch between the sugar contents measured at the

bulk leaf level and the amount of sugars actually available for metabolism within the guard cells, depending on the properties of the system responsible for sugar transport. For instance, the expression of *STP1* is enhanced at night but repressed by sugars (Stadler et al., 2003; Cordoba et al., 2015), making it possible that the sugar import system of the guard cells is out of phase with apoplastic sugar availability in the most severe starch mutants. Second, transient periods of carbon starvation may 'imprint' the metabolism or ion transport system of the guard cells, so that stomata are not able to respond to sugars immediately after resumption. Supporting this idea, critically low levels of sugars have strong effects on the diel transcriptome (Gibon et al., 2004b; Bläsing et al., 2005), and every night in *pgm* such starvation impacts gene expression and enzyme activities in the following day (Gibon et al., 2004a, 2004b). Starvation could then prevent stomatal movements, as observed in seedlings grown in plates, where very low carbon availability inactivates TARGET of RAPAMYCIN (TOR, a kinase involved in energy signalling), which leads to BAM1 inactivation, abolishment of starch degradation in the guard cells, and loss of endogenous stomatal rhythm (Han et al., 2022). However, neither *bam1* nor *amy3 bam1* had a discernible transpiration phenotype in our study, suggesting cell-autonomous starch breakdown is dispensable to maintain sugar homeostasis and endogenous rhythm in the guard cells of more mature plants. Overall, spatiotemporal uncoupling between sugar metabolism and stomatal movements may arise from different mechanisms, making it hard to predict the transpiration phenotype of a given mutant based on its starch turnover or sugar content in the absence of a quantitative, mechanistic model (Blatt et al., 2022).

In our conceptual framework, guard-cell starch does not drive diel stomatal movements but is one component of the metabolic network that contributes to, and is regulated by, sugar homeostasis in the guard cells. Interestingly, H^+-ATPase activity feedbacks on guard-cell starch. Notably, in the guard cells, H^+-ATPase activity is required for blue-light induced starch degradation and red-light induced starch synthesis, yet the mechanistic connections remains elusive (Blatt, 2016; Horrer et al., 2016; Flütsch et al., 2020b). Here, we unexpectedly observed that the guard cells of *mex1* are mainly devoid of starch. Whether this is a consequence of impaired H^+-ATPase activity remains unknown. Alternatively, MEX1 could have a direct impact on the synthesis of guard-cell starch, by

contributing to the import of carbohydrates from the cytosol to the chloroplast. It is thought that the import of triose-phosphate (triose-P) or of Glc6P from the cytosol through the triose-phosphate/phosphate translocator (TPT) or the glucose 6-phosphate/phosphate translocator (GPT) fuels starch synthesis in the guard cell chloroplasts (Overlach et al., 1993; Niewiadomski et al., 2005; Daloso et al., 2017; Flütsch et al., 2022; Figure 1A). Complementation experiments in *Escherichia coli* have shown that MEX1 from Arabidopsis is able to transport not only maltose but also glucose and Glc1P, while Glc6P was not tested (Findinier et al., 2017). Thus, we could conceive that MEX1 contributes to starch synthesis in the guard cells by importing cytosolic Glc6P. The possibility that guard-cell chloroplasts may also import Glc1P from the cytosol in the afternoon has been recently put forward, yet (Flütsch et al., 2022), but then the absence of guard-cell starch in *pgm* at the end of the day remains to be clarified. Beyond this speculation around sugar-phosphates, the activity of MEX1 may carry a lot of weight in the homeostasis of the guard cell metabolism, either through a direct subcellular compartmentation of some sugars or phosphate intermediates, or through an indirect feedback of maltose transport on the metabolic network. The fluxes of metabolites and ions between the different compartments of the cell are highly interlocked and critically important for CO_2- and light-induced stomatal movements (Shimazaki et al., 1989, 2007; Robaina-Estévez et al., 2017; Jezek et al., 2021; Lim et al., 2022), that were markedly disturbed in *mex1*. The *mex1* mutation may disturb this delicate metabolic equilibrium between organelles that normally enables proper stomatal behaviour – and starch synthesis in the guard cells.

To conclude, the circadian clock and carbon metabolism in the guard cells coordinates with H^+-ATPase activity and ion transport; stomatal movements then result from this dynamic equilibrium that mesophyll metabolism readily disturbs. Mechanistic integration is required to decipher these interactions.

METHODS

Plant material

Leaf starch metabolism in Arabidopsis is largely documented (Streb and Zeeman, 2012). All starch mutants used in this study were described previously and in the Col-0 background: *pgm*-1 (AT5G51820; Caspar et al., 1985), *pgi*-1 (AT4G24620; Yu et al., 2000), *isa1*-1 (AT2G39930; Delatte et al., 2005), *ss4*-3 (AT4G18240; Crumpton-Taylor et al., 2013), *sex1*-3 (AT1G10760; Caspar et al., 1991; Yu et al., 2001; Ritte et al., 2002), *amy3*-2 (AT1G69830; Yu et al., 2005), *bam1* (AT3G23920; Fulton et al., 2008), *bam3* (AT4G17090; Fulton et al., 2008), *amy3*-2 *bam1* (Horrer et al., 2016; Flütsch et al., 2020b), *bam1 bam3* (Fulton et al., 2008; Horrer et al., 2016; David et al., 2022), *mex1*-1 (AT5G17520; Niittylä et al., 2004), *dpe1*-2 (AT5G64860; Critchley et al., 2001) and *dpe2*-5 (AT2G40840; Chia et al., 2004). For sake of clarity, the allele number of the starch mutants has been omitted throughout the text and figures. Due to seed availability, the lines of *isa1*-1 and *ss4*-3 we used also contained a starvation reporter construct consisting of the promoter of the starvation gene AT1G10070 fused to luciferase coding sequence (*ProStarv::LUC*; Graf et al., 2010) that was inserted in the original mutants as well as in Col-0, as described by Crumpton-Taylor (2010). The transformed lines were denoted with a dagger throughout the figures. No difference in the transpiration pattern was observed between Col-0 and Col-0†. We also used two mutants affected in a guard cell malate transporter, *abcb14*-1 and *abcb14*-2 (AT1G28010; Lee et al., 2008).

Growth conditions

The plants were grown in the Phenopsis phenotyping platform (Granier et al., 2006). Arabidopsis seeds were sown in 200-ml cylindrical plastic pots filled with a weighed amount of soil, and then thinned to one plant per pot. Six to eight plants of each genotype were obtained. To analyse all genotypes on the same day while reducing differences in plant architecture arising from contrasting growth rates among genotypes, the sowing date was adapted for each genotype based on a preliminary experiment: *pgm*, *sex1* and *mex1* were sown 42 days before the experiment; *bam3*, *bam bam3*, *pgi*, *ss4*, *dpe1* and *dpe2* were sown 35 days before the experiment; and *bam1*, *amy3 bam1*,

amy3, *isa1*, *abcb14*-1, *abcb14*-2 and the wild-type plants were sown 28 days before the experiment. Plants were then grown under 12-h photoperiod at an irradiance of 180 µmol m^{-2} s^{-1}, with constant atmospheric CO_2 (400 ppm), air temperature (22°C) and relative humidity (60%) during day and night. Each pot was weighed daily and its soil water content kept constant (1.4 g water g^{-1} dry soil) by watering with a modified Hoagland solution.

The PhenoLeaks pipeline to monitor transpiration dynamics

Gravimetry experiment

Transpiration was measured by gravimetry. For the assay, the surface of each pot was covered with cellophane to prevent evaporation from the soil, and then with a plastic grid to facilitate further image analysis. The pots were maintained as such in the Phenopsis platform during 1.25 d. Then each pot was weighed at a frequency of about 30 min during 6.75 d by a moving scale (0.001 g precision, Precisa XB 620M, Precisa Instruments AG, Dietikon, Switzerland). When necessary, irrigation was performed manually using a syringae in order to maintain the target soil water content. During the first 2.75 d, environmental conditions were the same as during the growth period. At the start of the next day, atmospheric CO_2 was doubled to 800 ppm during the daytime, and returned to 400 ppm at night. At the start of the next day, irradiance was reduced to 50 µmol m^{-2} s^{-1} during the daytime. Then plants were given two days of recovery in the control, growth conditions. Environmental data were recorded together with the pot weights in a database (Fabre et al., 2011).

Data processing

The gravimetrical data were then processed using R scripts. Manual irrigation events and other outliers were detected by analysing the studentized residuals of a local linear regression model of pot weight loss against time. Afterwards, the regression was run again and individual pot transpiration was calculated at every 30 min (falling on the day/night transitions) as the fitted slope of the local linear relationship. Because moving linear regression inherently buffers rapid changes such as occurring during the day/night

transitions, we made sure that the time interval used for the local regression did not span these transitions. This was achieved by setting a variable interval depending on the current position in the day/night cycle: at the start of each day or night period, the interval was set to 90 min (~3 points), gradually increased to 360 min (~12 points) and then gradually decreased to 120 min (~4 points) at the end of the same period. This varying interval allowed us to achieve a satisfactory trade-off between temporal resolution at the day/night transitions and robustness elsewhere. The rate of water loss was corrected for plant growth to obtain transpiration per unit of projected leaf area. Leaf area was estimated by a linear or polynomial model (automatically selected for each plant depending on the fit quality) based on measurements of the daily projected surface extracted by image analysis.

Extraction of parameters

To quantify the dynamics, we extracted one set of parameters per plant and per environmental condition. For the control conditions, we first averaged the initial 2.75 d into a single 24-h kinetics. We computed the mean transpiration over 24-h (E_{diel}) and over each period (E_{day}, E_{night}), as well as dynamic parameters (Figure 3A). We estimated the diel amplitude of transpiration (A_{diel}), the time of maximal daytime transpiration ($t_{day\ max}$), the cumulative afternoon preclosure after $t_{day\ max}$ (Σ_{preclo}), the time of minimal nighttime transpiration ($t_{night\ min}$) and the cumulative nighttime preopening after $t_{night\ min}$ (Σ_{preop}). Then, we separated the rapid changes observed at the day/night transitions from the endogenous changes of the rest of each period. The exponential response of stomata to a rapid change in light intensity have largely plateaued after 30 min (Matthews et al., 2018). Even in “delayed genotypes” such as *pgm* and *mex1*, the changes observed after 30 min were not quantitatively consistent with a prolongation of the exponential kinetics. Therefore, the magnitude of rapid opening at the night-to-day-transition ($A_{rapid\ op}$) and that of the rapid closure at the day-to-night transition ($A_{rapid\ clo}$) were estimated at 30 min after a transition. Finally, we estimated the average slope of change in transpiration throughout the daytime after 30-min illumination (σ_{day}), the cumulative transpiration dynamics above this daytime trend during the same period (Δ_{day}, usually positive; the area below the trend, if any, being subtracted), the average

slope of change in transpiration throughout the nighttime after 30-min darkness (σ_{night}) and the cumulative transpiration dynamics below this nighttime trend during the same period (Δ_{night}, usually negative; the area above the trend, if any, being added). The same procedure was applied on the fitted curves, and the obtained parameters were denoted with a hat (Figure 4B). Cumulative parameters were obtained through trapezoidal integration for the measured data (Σ_{preclo}, Σ_{preop}, Δ_{day}, Δ_{night}), and by calculating primitive integrals for the fitted curves ($\widehat{\Sigma}_{preclo}$, $\widehat{\Sigma}_{preop}$, $\widehat{\Delta}_{day}$, $\widehat{\Delta}_{night}$).

The code will be made available as R scripts on the PhenoLeaks repository (GitHub). The link will be provided upon publication of the manuscript in a peer-reviewed journal.

Modelling the diel transpiration dynamics

Model structure

To model the transpiration dynamics, we used a periodic signal (Figure 4A) composed of a square wave (period fixed to 24 h, semi-amplitude A_{SQW}, phase ε), a fundamental sine wave (period fixed to 24 h, semi-amplitude A_1, phase φ_1) and its second harmonic (period fixed to 12 h, semi-amplitude A_2, phase φ_2) that oscillates around a baseline transpiration (E_{mean}):

$$\widehat{E} = E_{mean} + A_{SQW}\,\mathrm{sgn}\left(\sin\left((t+\varepsilon)\times 2\pi\right)\right) + A_1 \sin\left(\left(t+\varphi_1\right)\times 2\pi\right) + A_2 \sin\left(\left(t+\varphi_2\right)\times 4\pi\right)$$

with t the time ($t = 0$ being the start of the first day period) and sgn() the signum function. We shifted the phase of the square wave by $\varepsilon = -15$ min (*i.e.* the square wave lags 15 min behind the day/night transitions) so that the square wave is worth $+A_{SQW}$ during the day and at the day-to-night transition, $-A_{SQW}$ during the night and at the night-to-day transition, and 0 at 15 min after the transitions (when there is no data to be fitted since transpiration is estimated at every 30 min starting from 0).

Model fitting

To fit the model to the data, we transformed the model so that it can be fitted used multiple linear regression:

$$\hat{E} = E_{mean} + A_{SQW}\,\mathrm{sgn}\left(\sin\left((t+\varepsilon)\times 2\pi\right)\right) + a_1 \sin(2\pi t) + b_1 \cos(2\pi t) + a_2 \sin(4\pi t) + b_2 \cos(4\pi t)$$

with:

$$A_i = \sqrt{a_i^2 + b_i^2}\ ;\ i \in \{1\ ;\ 2\}$$

and

$$\varphi_i = \begin{cases} \tan^{-1}\left(\frac{b_i}{a_i}\right) & \text{if } a_i > 0 \\ \tan^{-1}\left(\frac{b_i}{a_i}\right) + \pi & \text{otherwise} \end{cases}\ ;\ i \in \{1\ ;\ 2\}$$

Once the parameters were obtained, the phases were wrapped so that $-12\ \mathrm{h} < \varphi_1 \leq +12\ \mathrm{h}$ and $-6\ \mathrm{h} < \varphi_2 \leq +6\ \mathrm{h}$.

For each plant, a set of parameters was obtained using data from the interval [–0.75 d ; 2 d] for the control conditions,]2 d ; 3 d] for elevated CO_2,]3 d ; 4 d] for low irradiance,]4 d ; 5 d] for recovery day one, and]5 d ; 6 d] for recovery day two. Thus, each condition was parameterized independently of the previous one, and for non-control conditions the square wave was only constrained by the day-to-night transition. Moreover, for the fit, we systematically excluded the data at 0 and 30 min after the transitions to avoid two potential biases when estimating the parameters: first, measurement uncertainty around these points was higher due to the shorter time interval used at the transitions when performing the floating linear regression (see previous section); second, the point at 30 min after the transition might be affected by a slower exponential response of stomata to a rapid change in irradiance (Matthews et al., 2018) or by transient hydromechanical effects of the epidermal cells on stomata (Jezek et al., 2019). This enabled suppressing a few outliers, but did not affect the conclusions of the manuscript.

The code will be made available as R scripts on the PhenoLeaks repository (GitHub). The link will be provided upon publication of the manuscript in a peer-reviewed journal.

Gas exchange for maltose feeding assays

Gas exchange experiments were performed on xylem-fed detached leaves as described previously (Pantin et al., 2013a). Mature leaves of Col-0 plants were excised one hour before the end of the night period (darkness experiment) or during the daytime (light experiment), and immediately recut under water. The petiole was then dipped in an Eppendorf containing water and the leaf was inserted into a 2×3 LED chamber of a Li6400-XT infrared gas analyser (Li-Cor Inc., Lincoln, NE, USA) connected to a Li610 dew-point generator (Li-Cor Inc.), and data were logged every 10 s. CO_2 was set at 400 ppm, block temperature at 22°C and reference dew-point temperature at 17°C. Irradiance was set at either 0, 50, 200 or 500 µmol m^{-2} s^{-1} depending on the experiment. Once stomatal conductance had stabilized, water was changed against a 1 mM maltose solution. For the maltose effect at the dark-to-light transition, leaves were harvested at the end of the night, dipped into 1 mM maltose or water (control) for at least 2 h in darkness before monitoring gas exchange at the dark-to-light transition.

Starch analyses

During the transpiration assay, leaf samples for starch analysis were obtained at the end of the day and night periods on distinct plants. Four biological replicates were harvested per genotype at each time point. Approximately 40 mg of fresh leaf material per rosette was harvested, weighed and immediately frozen in liquid nitrogen. Starch content was analysed by enzymatic assay using spectrophotometric analysis of the residual fraction of ethanol-water extracts (Hummel et al., 2010).

For iodine staining of starch, leaves were harvested and decolourised in 80% (v/v) ethanol. Excess of ethanol was removed by rinsing with water. Leaves were stained with a 30% (v/v) lugol solution for 30 min followed by a wash step of 30 min with water. The iodine staining was observed using an Olympus BX61 (60x, guard cells) and SZX16 (0.5x, whole leaves) microscope.

Statistical analyses

Data management, statistical analyses and figures were produced using R 4.2.0 (R Development Core Team, 2022). Differences in starch contents were analysed using the Kruskal-Wallis non-parametric test at the 5% level followed by multiple comparisons of the ranks through Fisher's LSD adjusted by the Benjamini-Hochberg method (de Mendiburu, 2021). The parameters extracted from the transpiration dynamics were analysed using two-way mixed ANOVA (genotype being the between-subjects factor, and environment the within-subjects factor), where the effect sizes of both factors and their interaction were computed using the generalized eta squared (η^2_g), which was followed by pairwise t-tests adjusted by the Bonferroni method (Kassambara, 2021). The figures systematically show the significant differences between genotypes for each environment. When required, similar tests were carried out to test the significance of the differences between environments, which was reported in the main text. For the heatmap, hierarchical clustering analysis was done with the complete method using the Euclidean distances on scaled and centred data (Gu, 2022).

Accession numbers

Sequence data from this article can be found in the EMBL/GenBank data libraries under accession numbers AT5G51820 (*PGM*), AT4G24620 (*PGI*), AT1G10760 (*SEX1*/*GWD*), AT1G69830 (*AMY3*), AT3G23920 (*BAM1*), AT4G17090 (*BAM3*), AT5G17520 (*MEX1*), AT5G64860 (*DPE1*), AT2G40840 (*DPE2*), AT4G18240 (*SS4*), AT2G39930 (*ISA1*) and AT1G28010 (*ABCB14*).

Supplemental data

Supplemental Figure S1. Comparison of further transpiration parameters for *pgm* and *sex1*.

Supplemental Figure S2. Comparison of further transpiration parameters for *isa1* and *ss4*.

Supplemental Figure S3. Comparison of further transpiration parameters for *mex1*, *dpe1* and *dpe2*.

Supplemental Figure S4. Effect of exogenous maltose on stomatal conductance of Col-0.

Supplemental Figure S5. Comparison of further transpiration parameters for *pgi*, *amy3 bam1* and *bam1 bam3*.

Supplemental Figure S6. Analysis of diel transpiration of *amy3*, *bam1* and *bam3* single mutants.

Supplemental Figure S7. Comparison of further transpiration parameters for *amy3*, *bam1* and *bam3*.

Supplemental Figure S8. Characterization of the starch patterns in *abcb14*-1 and *abcb14*-2.

Supplemental Figure S9. Comparison of further transpiration parameters for *abcb14*-1 and *abcb14*-2.

ACKNOWLEDGEMENTS

We thank Jérémy Cortello and Alexis Bédiée for technical help during the transpiration experiments, Gaëlle Rolland for assistance during starch measurements, Carine Alcon for guidance in microscopy, Anna Medici for advices on genotyping, and the groups of Samuel C. Zeeman and Youngsook Lee for providing seeds of starch and *abcb14* mutants, respectively. We are grateful to Alison M. Smith and Doreen Feike for the gift of the LUC-expressing lines and advice on their analysis. This research was supported by INRAE and Région Occitanie (PhD fellowship to A.J.W.).

AUTHOR CONTRIBUTIONS

FP, TS and AJW designed the research; AJW and MD performed the transpiration experiments; FP performed the gas exchange experiments; AJW and FP developed PhenoLeaks; FP developed the model; AJW and FP analyzed data; FP wrote the draft of the paper; AJW and TS revised the manuscript.

REFERENCES

Ando, E., Ohnishi, M., Wang, Y., Matsushita, T., Watanabe, A., Hayashi, Y., Fujii, M., Ma, J.F., Inoue, S., and Kinoshita, T. (2013). *TWIN SISTER OF FT*, *GIGANTEA*, and *CONSTANS* have a positive but indirect effect on blue light-induced stomatal opening in Arabidopsis. Plant Physiol. 162: 1529–1538.

Apelt, F., Breuer, D., Nikoloski, Z., Stitt, M., and Kragler, F. (2015). Phytotyping^{4D}: a light-field imaging system for non-invasive and accurate monitoring of spatio-temporal plant growth. Plant J. 82: 693–706.

Araújo, W.L., Tohge, T., Ishizaki, K., Leaver, C.J., and Fernie, A.R. (2011). Protein degradation - an alternative respiratory substrate for stressed plants. Trends Plant Sci. 16: 489–498.

Azoulay-Shemer, T., Bagheri, A., Wang, C., Palomares, A., Stephan, A.B., Kunz, H.-H., and Schroeder, J.I. (2016). Starch biosynthesis in guard cells but not in mesophyll cells is involved in CO_2-induced stomatal closing. Plant Physiol. 171: 788–798.

Azoulay-Shemer, T., Palomares, A., Bagheri, A., Israelsson-Nordstrom, M., Engineer, C.B., Bargmann, B.O.R., Stephan, A.B., and Schroeder, J.I. (2015). Guard cell photosynthesis is critical for stomatal turgor production, yet does not directly mediate CO_2- and ABA-induced stomatal closing. Plant J. 83: 567–581.

Azoulay-Shemer, T., Schwankl, N., Rog, I., Moshelion, M., and Schroeder, J.I. (2018). Starch biosynthesis by AGPase, but not starch degradation by BAM1/3 and SEX1, is rate-limiting for CO_2-regulated stomatal movements under short-day conditions. FEBS Lett. 592: 2739–2759.

Bläsing, O.E., Gibon, Y., Günther, M., Höhne, M., Morcuende, R., Osuna, D., Thimm, O., Usadel, B., Scheible, W.-R., and Stitt, M. (2005). Sugars and circadian regulation make major contributions to the global regulation of diurnal gene expression in *Arabidopsis*. Plant Cell 17: 3257–3281.

Blatt, M.R. (2016). Plant physiology: redefining the enigma of metabolism in stomatal movement. Curr. Biol. 26: R107–R109.

Blatt, M.R., Jezek, M., Lew, V.L., and Hills, A. (2022). What can mechanistic models tell us about guard cells, photosynthesis, and water use efficiency? Trends Plant Sci. 27: 166–179.

Blatt, M.R., Wang, Y., Leonhardt, N., and Hills, A. (2014). Exploring emergent properties in cellular homeostasis using OnGuard to model K^+ and other ion transport in guard cells. J. Plant Physiol. 171: 770–778.

Caird, M.A., Richards, J.H., and Donovan, L.A. (2007). Nighttime stomatal conductance and transpiration in C_3 and C_4 plants. Plant Physiol. 143: 4–10.

Caspar, T., Huber, S.C., and Somerville, C.R. (1985). Alterations in growth, photosynthesis, and respiration in a starchless mutant of *Arabidopsis thaliana* (L.) deficient in chloroplast phosphoglucomutase activity. Plant Physiol. 79: 11–17.

Caspar, T., Lin, T.-P., Kakefuda, G., Benbow, L., Preiss, J., and Somerville, C.R. (1991). Mutants of *Arabidopsis* with altered regulation of starch degradation. Plant Physiol. 95: 1181–1188.

Chia, T., Thorneycroft, D., Chapple, A., Messerli, G., Chen, J., Zeeman, S.C., Smith, S.M., and Smith, A.M. (2004). A cytosolic glucosyltransferase is required for conversion of starch to sucrose in *Arabidopsis* leaves at night. Plant J. 37: 853–863.

Cho, M.-H., Lim, H., Shin, D.H., Jeon, J.-S., Bhoo, S.H., Park, Y.-I., and Hahn, T.-R. (2011). Role of the plastidic glucose translocator in the export of starch degradation products from the chloroplasts in *Arabidopsis thaliana*. New Phytol. 190: 101–112.

Cordoba, E., Aceves-Zamudio, D.L., Hernández-Bernal, A.F., Ramos-Vega, M., and León, P. (2015). Sugar regulation of *SUGAR TRANSPORTER PROTEIN 1* (*STP1*) expression in *Arabidopsis thaliana*. J. Exp. Bot. 66: 147–159.

Costa, J.M., Monnet, F., Jannaud, D., Leonhardt, N., Ksas, B., Reiter, I.M., Pantin, F., and Genty, B. (2015). *OPEN ALL NIGHT LONG*: the dark side of stomatal control. Plant Physiol. 167: 289–294.

Coupel-Ledru, A., Lebon, E., Christophe, A., Gallo, A., Gago, P., Pantin, F., Doligez, A., and Simonneau, T. (2016). Reduced nighttime transpiration is a relevant breeding target for high water-use efficiency in grapevine. Proc. Natl. Acad. Sci. U. S. A. 113: 8963–8968.

Critchley, J.H., Zeeman, S.C., Takaha, T., Smith, A.M., and Smith, S.M. (2001). A critical role for disproportionating enzyme in starch breakdown is revealed by a knock-out mutation in *Arabidopsis*. Plant J. 26: 89–100.

Crumpton-Taylor, M. (2010). Starch granule number and size in *Arabidopsis thaliana* leaves.

Crumpton-Taylor, M., Pike, M., Lu, K.-J., Hylton, C.M., Feil, R., Eicke, S., Lunn, J.E., Zeeman, S.C., and Smith, A.M. (2013). Starch synthase 4 is essential for coordination of starch granule formation with chloroplast division during Arabidopsis leaf expansion. New Phytol. 200: 1064–1075.

Dakhiya, Y. and Green, R.M. (2019). Thermal imaging as a noninvasive technique for analyzing circadian rhythms in plants. New Phytol. 224: 1685–1696.

Dalchau, N., Baek, S.J., Briggs, H.M., Robertson, F.C., Dodd, A.N., Gardner, M.J., Stancombe, M.A., Haydon, M.J., Stan, G.-B., Gonçalves, J.M., and Webb, A.A.R. (2011). The

circadian oscillator gene *GIGANTEA* mediates a long-term response of the *Arabidopsis thaliana* circadian clock to sucrose. Proc. Natl. Acad. Sci. U. S. A. 108: 5104–5109.

Daloso, D.M., dos Anjos, L., and Fernie, A.R. (2016a). Roles of sucrose in guard cell regulation. New Phytol. 211: 809–818.

Daloso, D.M., Antunes, W.C., Pinheiro, D.P., Waquim, J.P., Araújo, W.L., Loureiro, M.E., Fernie, A.R., and Williams, T.C.R. (2015). Tobacco guard cells fix CO_2 by both Rubisco and PEPcase while sucrose acts as a substrate during light-induced stomatal opening. Plant Cell Environ. 38: 2353–2371.

Daloso, D.M., Medeiros, D.B., dos Anjos, L., Yoshida, T., Araújo, W.L., and Fernie, A.R. (2017). Metabolism within the specialized guard cells of plants. New Phytol. 216: 1018–1033.

Daloso, D.M., Williams, T.C.R., Antunes, W.C., Pinheiro, D.P., Müller, C., Loureiro, M.E., and Fernie, A.R. (2016b). Guard cell-specific upregulation of *sucrose synthase 3* reveals that the role of sucrose in stomatal function is primarily energetic. New Phytol. 209: 1470–1483.

David, L.C., Lee, S.-K., Bruderer, E., Abt, M.R., Fischer-Stettler, M., Tschopp, M.-A., Solhaug, E.M., Sanchez, K., and Zeeman, S.C. (2022). BETA-AMYLASE9 is a plastidial nonenzymatic regulator of leaf starch degradation. Plant Physiol. 188: 191–207.

Delatte, T., Trevisan, M., Parker, M.L., and Zeeman, S.C. (2005). Arabidopsis mutants *Atisa1* and *Atisa2* have identical phenotypes and lack the same multimeric isoamylase, which influences the branch point distribution of amylopectin during starch synthesis. Plant J. 41: 815–830.

Dittrich, P. and Mayer, M. (1978). Inhibition of stomatal opening during uptake of carbohydrates by guard cells in isolated epidermal tissues. Planta 139: 167–170.

Dittrich, P. and Raschke, K. (1977). Uptake and metabolism of carbohydrates by epidermal tissue. Planta 134: 83–90.

Dodd, A.N., Parkinson, K., and Webb, A.A.R. (2004). Independent circadian regulation of assimilation and stomatal conductance in the *ztl-1* mutant of *Arabidopsis*. New Phytol. 162: 63–70.

Dodd, A.N., Salathia, N., Hall, A., Kévei, E., Tóth, R., Nagy, F., Hibberd, J.M., Millar, A.J., and Webb, A.A.R. (2005). Plant circadian clocks increase photosynthesis, growth, survival, and competitive advantage. Science 309: 630–633.

Easlon, H.M. and Richards, J.H. (2009). Photosynthesis affects following night leaf conductance in *Vicia faba*. Plant Cell Environ. 32: 58–63.

Endo, M. (2016). Tissue-specific circadian clocks in plants. Curr. Opin. Plant Biol. 29: 44–49.

Eyland, D., van Wesemael, J., Lawson, T., and Carpentier, S. (2021). The impact of slow stomatal kinetics on photosynthesis and water use efficiency under fluctuating light. Plant Physiol. 186: 998–1012.

Fabre, J., Dauzat, M., Nègre, V., Wuyts, N., Tireau, A., Gennari, E., Neveu, P., Tisné, S., Massonnet, C., Hummel, I., and Granier, C. (2011). PHENOPSIS DB: an Information System for *Arabidopsis thaliana* phenotypic data in an environmental context. BMC Plant Biol. 11: 77.

Findinier, J. et al. (2017). The *Chlamydomonas mex1* mutant shows impaired starch mobilization without maltose accumulation. J. Exp. Bot. 68: 5177–5189.

Flütsch, S., Horrer, D., and Santelia, D. (2022). Starch biosynthesis in guard cells has features of both autotrophic and heterotrophic tissues. Plant Physiol. 189: 541–556.

Flütsch, S., Nigro, A., Conci, F., Fajkus, J., Thalmann, M., Trtílek, M., Panzarová, K., and Santelia, D. (2020a). Glucose uptake to guard cells via STP transporters provides carbon sources for stomatal opening and plant growth. EMBO Rep. 21: e49719.

Flütsch, S. and Santelia, D. (2021). Mesophyll-derived sugars are positive regulators of light-driven stomatal opening. New Phytol. 230: 1754–1760.

Flütsch, S., Wang, Y., Takemiya, A., Vialet-Chabrand, S.R.M., Klejchová, M., Nigro, A., Hills, A., Lawson, T., Blatt, M.R., and Santelia, D. (2020b). Guard cell starch degradation yields glucose for rapid stomatal opening in Arabidopsis. Plant Cell 32: 2325–2344.

Frank, A. et al. (2018). Circadian entrainment in *Arabidopsis* by the sugar-responsive transcription factor bZIP63. Curr. Biol. 28: 2597-2606.e6.

Fulton, D.C. et al. (2008). β-AMYLASE4, a noncatalytic protein required for starch breakdown, acts upstream of three active β-amylases in *Arabidopsis* chloroplasts. Plant Cell 20: 1040–1058.

Gibon, Y., Bläsing, O.E., Hannemann, J., Carillo, P., Höhne, M., Hendriks, J.H.M., Palacios, N., Cross, J.M., Selbig, J., and Stitt, M. (2004a). A robot-based platform to measure multiple enzyme activities in Arabidopsis using a set of cycling assays: comparison of changes of enzyme activities and transcript levels during diurnal cycles and in prolonged darkness. Plant Cell 16: 3304–3325.

Gibon, Y., Bläsing, O.E., Palacios-Rojas, N., Pankovic, D., Hendriks, J.H.M., Fisahn, J., Höhne, M., Günther, M., and Stitt, M. (2004b). Adjustment of diurnal starch turnover to short days: depletion of sugar during the night leads to a temporary inhibition of carbohydrate utilization, accumulation of sugars and post-translational activation of ADP-glucose pyrophosphorylase in the following light period. Plant J. 39: 847–862.

Graf, A., Schlereth, A., Stitt, M., and Smith, A.M. (2010). Circadian control of carbohydrate availability for growth in *Arabidopsis* plants at night. Proc. Natl. Acad. Sci. U. S. A. 107: 9458–9463.

Granier, C. et al. (2006). PHENOPSIS, an automated platform for reproducible phenotyping of plant responses to soil water deficit in *Arabidopsis thaliana* permitted the identification of an accession with low sensitivity to soil water deficit. New Phytol. 169: 623–635.

Granot, D. and Kelly, G. (2019). Evolution of guard-cell theories: the story of sugars. Trends Plant Sci. 24: 507–518.

Gu, Z. (2022). Complex heatmap visualization. iMeta 1: e43.

Han, C., Hua, W., Li, J., Qiao, Y., Yao, L., Hao, W., Li, R., Fan, M., De Jaeger, G., Yang, W., and Bai, M.-Y. (2022). TOR promotes guard cell starch degradation by regulating the activity of β-AMYLASE1 in Arabidopsis. Plant Cell 34: 1038–1053.

Hassidim, M., Dakhiya, Y., Turjeman, A., Hussien, D., Shor, E., Anidjar, A., Goldberg, K., and Green, R.M. (2017). *CIRCADIAN CLOCK ASSOCIATED 1* (*CCA1*) and the circadian control of stomatal aperture. Plant Physiol. 175: 1864–1877.

Haydon, M.J., Mielczarek, O., Frank, A., Román, Á., and Webb, A.A.R. (2017). Sucrose and ethylene signaling interact to modulate the circadian clock. Plant Physiol. 175: 947–958.

Haydon, M.J., Mielczarek, O., Robertson, F.C., Hubbard, K.E., and Webb, A.A.R. (2013). Photosynthetic entrainment of the *Arabidopsis thaliana* circadian clock. Nature 502: 689–692.

Hetherington, A.M. and Woodward, F.I. (2003). The role of stomata in sensing and driving environmental change. Nature 424: 901–908.

Hõrak, H., Fountain, L., Dunn, J.A., Landymore, J., and Gray, J.E. (2021). Dynamic thermal imaging confirms local but not fast systemic ABA responses. Plant Cell Environ. 44: 885–899.

Horrer, D., Flütsch, S., Pazmino, D., Matthews, J.S.A., Thalmann, M., Nigro, A., Leonhardt, N., Lawson, T., and Santelia, D. (2016). Blue light induces a distinct starch degradation pathway in guard cells for stomatal opening. Curr. Biol. 26: 362–370.

Hubbard, K.E. and Webb, A.A.R. (2011). Circadian rhythms: *FLOWERING LOCUS T* extends opening hours. Curr. Biol. 21: R636–R638.

Hubbard, K.E. and Webb, A.A.R. (2015). Circadian rhythms in stomata: physiological and molecular aspects. In Rhythms in Plants: Dynamic Responses in a Dynamic Environment, S. Mancuso and S. Shabala, eds (Springer International Publishing: Cham, Switzerland), pp. 231–255.

Hughes, M.E., DiTacchio, L., Hayes, K.R., Vollmers, C., Pulivarthy, S., Baggs, J.E., Panda, S., and Hogenesch, J.B. (2009). Harmonics of circadian gene transcription in mammals. PLoS Genet. 5: e1000442.

Hummel, I., Pantin, F., Sulpice, R., Piques, M., Rolland, G., Dauzat, M., Christophe, A., Pervent, M., Bouteillé, M., Stitt, M., Gibon, Y., and Muller, B. (2010). Arabidopsis plants acclimate to water deficit at low cost through changes of carbon usage: an integrated perspective using growth, metabolite, enzyme, and gene expression analysis. Plant Physiol. 154: 357–372.

Jezek, M. and Blatt, M.R. (2017). The membrane transport system of the guard cell and its integration for stomatal dynamics. Plant Physiol. 174: 487–519.

Jezek, M., Hills, A., Blatt, M.R., and Lew, V.L. (2019). A constraint–relaxation–recovery mechanism for stomatal dynamics. Plant Cell Environ. 42: 2399–2410.

Jezek, M., Silva-Alvim, F.A.L., Hills, A., Donald, N., Ishka, M.R., Shadbolt, J., He, B., Lawson, T., Harper, J.F., Wang, Y., Lew, V.L., and Blatt, M.R. (2021). Guard cell endomembrane Ca^{2+}-ATPases underpin a 'carbon memory' of photosynthetic assimilation that impacts on water-use efficiency. Nat. Plants 7: 1301–1313.

Kane, C.N., Jordan, G.J., Jansen, S., and McAdam, S.A.M. (2020). A permeable cuticle, not open stomata, is the primary source of water loss from expanding leaves. Front. Plant Sci. 11: 774.

Kassambara, A. (2021). rstatix: Pipe-friendly framework for basic statistical tests. R package version 0.7.0.

Kelly, G., Egbaria, A., Khamaisi, B., Lugassi, N., Attia, Z., Moshelion, M., and Granot, D. (2019). Guard-cell hexokinase increases water-use efficiency under normal and drought conditions. Front. Plant Sci. 10: 1499.

Kelly, G., Moshelion, M., David-Schwartz, R., Halperin, O., Wallach, R., Attia, Z., Belausov, E., and Granot, D. (2013). Hexokinase mediates stomatal closure. Plant J. 75: 977–988.

Kinoshita, T., Ono, N., Hayashi, Y., Morimoto, S., Nakamura, S., Soda, M., Kato, Y., Ohnishi, M., Nakano, T., Inoue, S., and Shimazaki, K. (2011). *FLOWERING LOCUS T* regulates stomatal opening. Curr. Biol. 21: 1232–1238.

Kunz, H.H., Häusler, R.E., Fettke, J., Herbst, K., Niewiadomski, P., Gierth, M., Bell, K., Steup, M., Flügge, U.I., and Schneider, A. (2010). The role of plastidial glucose-6-phosphate/phosphate translocators in vegetative tissues of *Arabidopsis thaliana* mutants impaired in starch biosynthesis. Plant Biol. 12 (Suppl. 1): 115–128.

Lascève, G., Leymarie, J., and Vavasseur, A. (1997). Alterations in light-induced stomatal opening in a starch-deficient mutant of *Arabidopsis thaliana* L. deficient in chloroplast phosphoglucomutase activity. Plant Cell Environ. 20: 350–358.

Lawson, T. and Blatt, M.R. (2014). Stomatal size, speed, and responsiveness impact on photosynthesis and water use efficiency. Plant Physiol. 164: 1556–1570.

Lawson, T. and Matthews, J. (2020). Guard cell metabolism and stomatal function. Annu. Rev. Plant Biol. 71: 273–302.

Lebaudy, A., Vavasseur, A., Hosy, E., Dreyer, I., Leonhardt, N., Thibaud, J.-B., Véry, A.-A., Simonneau, T., and Sentenac, H. (2008). Plant adaptation to fluctuating environment and biomass production are strongly dependent on guard cell potassium channels. Proc. Natl. Acad. Sci. U. S. A. 105: 5271–5276.

Lee, M., Choi, Y., Burla, B., Kim, Y.-Y., Jeon, B., Maeshima, M., Yoo, J.-Y., Martinoia, E., and Lee, Y. (2008). The ABC transporter AtABCB14 is a malate importer and modulates stomatal response to CO_2. Nat. Cell Biol. 10: 1217–1223.

Leymarie, J., Lascève, G., and Vavasseur, A. (1998). Interaction of stomatal responses to ABA and CO_2 in *Arabidopsis thaliana*. Aust. J. Plant Physiol. 25: 785–791.

Li, D. et al. (2020). Daily rhythms of phytomelatonin signaling modulate diurnal stomatal closure via regulating reactive oxygen species dynamics in *Arabidopsis*. J. Pineal Res. 68: e12640.

Lim, S.-L., Flütsch, S., Liu, J., Distefano, L., Santelia, D., and Lim, B.L. (2022). Arabidopsis guard cell chloroplasts import cytosolic ATP for starch turnover and stomatal opening. Nat. Commun. 13: 652.

Loftfield, J.V.G. (1921). The behavior of stomata (Carnegie Institution of Washington: Washington, USA).

Lu, K.-J., Pfister, B., Jenny, C., Eicke, S., and Zeeman, S.C. (2018). Distinct functions of STARCH SYNTHASE 4 domains in starch granule formation. Plant Physiol. 176: 566–581.

Lu, P., Outlaw, W.H., Jr., Smith, B.G., and Freed, G.A. (1997). A new mechanism for the regulation of stomatal aperture size in intact leaves. Accumulation of mesophyll-derived sucrose in the guard-cell wall of *Vicia faba*. Plant Physiol. 114: 109–118.

Lu, Y., Gehan, J.P., and Sharkey, T.D. (2005). Daylength and circadian effects on starch degradation and maltose metabolism. Plant Physiol. 138: 2280–2291.

Lu, Y. and Sharkey, T.D. (2004). The role of amylomaltase in maltose metabolism in the cytosol of photosynthetic cells. Planta 218: 466–473.

Lu, Y., Steichen, J.M., Weise, S.E., and Sharkey, T.D. (2006). Cellular and organ level localization of maltose in maltose-excess *Arabidopsis* mutants. Planta 224: 935–943.

Lugassi, N., Kelly, G., Fidel, L., Yaniv, Y., Attia, Z., Levi, A., Alchanatis, V., Moshelion, M., Raveh, E., Carmi, N., and Granot, D. (2015). Expression of *Arabidopsis* hexokinase in citrus guard cells controls stomatal aperture and reduces transpiration. Front. Plant Sci. 6: 1114.

Martins, B.M.C., Das, A.K., Antunes, L., and Locke, J.C.W. (2016). Frequency doubling in the cyanobacterial circadian clock. Mol. Syst. Biol. 12: 896.

Matthews, J.S.A., Vialet-Chabrand, S.R.M., and Lawson, T. (2018). Acclimation to fluctuating light impacts the rapidity of response and diurnal rhythm of stomatal conductance. Plant Physiol. 176: 1939–1951.

de Mendiburu, F. (2021). agricolae: Statistical procedures for agricultural research. R package version 1.3-5.

Merlot, S., Leonhardt, N., Fenzi, F., Valon, C., Costa, M., Piette, L., Vavasseur, A., Genty, B., Boivin, K., Müller, A., Giraudat, J., and Leung, J. (2007). Constitutive activation of a plasma membrane H^+-ATPase prevents abscisic acid-mediated stomatal closure. EMBO J. 26: 3216–3226.

Nieves-Cordones, M. et al. (2022). Non-autonomous stomatal control by pavement cell turgor via the K^+ channel subunit *AtKC1*. Plant Cell 34: 2019–2037.

Niewiadomski, P., Knappe, S., Geimer, S., Fischer, K., Schulz, B., Unte, U.S., Rosso, M.G., Ache, P., Flügge, U.-I., and Schneider, A. (2005). The Arabidopsis plastidic glucose 6-phosphate/phosphate translocator GPT1 is essential for pollen maturation and embryo sac development. Plant Cell 17: 760–775.

Niittylä, T., Messerli, G., Trevisan, M., Chen, J., Smith, A.M., and Zeeman, S.C. (2004). A previously unknown maltose transporter essential for starch degradation in leaves. Science 303: 87–89.

Outlaw, W.H., Jr. and Manchester, J. (1979). Guard cell starch concentration quantitatively related to stomatal aperture. Plant Physiol. 64: 79–82.

Overlach, S., Diekmann, W., and Raschke, K. (1993). Phosphate translocator of isolated guard-cell chloroplasts from *Pisum sativum* L. transports glucose-6-phosphate. Plant Physiol. 101: 1201–1207.

Pal, S.K. et al. (2013). Diurnal changes of polysome loading track sucrose content in the rosette of wild-type Arabidopsis and the starchless *pgm* mutant. Plant Physiol. 162: 1246–1265.

Pantin, F., Monnet, F., Jannaud, D., Costa, J.M., Renaud, J., Muller, B., Simonneau, T., and Genty, B. (2013a). The dual effect of abscisic acid on stomata. New Phytol. 197: 65–72.

Pantin, F., Renaud, J., Barbier, F., Vavasseur, A., Le Thiec, D., Rose, C., Bariac, T., Casson, S., McLachlan, D.H., Hetherington, A.M., Muller, B., and Simonneau, T. (2013b). Developmental priming of stomatal sensitivity to abscisic acid by leaf microclimate. Curr. Biol. 23: 1805–1811.

Papanatsiou, M., Petersen, J., Henderson, L., Wang, Y., Christie, J.M., and Blatt, M.R. (2019). Optogenetic manipulation of stomatal kinetics improves carbon assimilation, water use, and growth. Science 363: 1456–1459.

Plautz, J.D., Straume, M., Stanewsky, R., Jamison, C.F., Brandes, C., Dowse, H.B., Hall, J.C., and Kay, S.A. (1997). Quantitative analysis of *Drosophila period* gene transcription in living animals. J. Biol. Rhythms 12: 204–217.

Poffenroth, M., Green, D.B., and Tallman, G. (1992). Sugar concentrations in guard cells of *Vicia faba* illuminated with red or blue light. Analysis by high performance liquid chromatography. Plant Physiol. 98: 1460–1471.

R Development Core Team (2022). R: A language and environment for statistical computing.

Ritte, G., Lloyd, J.R., Eckermann, N., Rottmann, A., Kossmann, J., and Steup, M. (2002). The starch-related R1 protein is an *α*-glucan, water dikinase. Proc. Natl. Acad. Sci. U. S. A. 99: 7166–7171.

Robaina-Estévez, S., Daloso, D.M., Zhang, Y., Fernie, A.R., and Nikoloski, Z. (2017). Resolving the central metabolism of Arabidopsis guard cells. Sci. Rep. 7: 8307.

Roldán, I., Wattebled, F., Lucas, M.M., Delvallé, D., Planchot, V., Jiménez, S., Pérez, R., Ball, S., D'Hulst, C., and Mérida, Á. (2007). The phenotype of soluble starch synthase IV defective mutants of Arabidopsis thaliana suggests a novel function of elongation enzymes in the control of starch granule formation. Plant J. 49: 492–504.

Santelia, D. and Lawson, T. (2016). Rethinking guard cell metabolism. Plant Physiol. 172: 1371–1392.

Santelia, D. and Lunn, J.E. (2017). Transitory starch metabolism in guard cells: unique features for a unique function. Plant Physiol. 174: 539–549.

Schwabe, W.W. (1952). Effects of photoperiodic treatment on stomatal movement. Nature 169: 1053–1054.

Seki, M., Ohara, T., Hearn, T.J., Frank, A., Silva, V.C.H., Caldana, C., Webb, A.A.R., and Satake, A. (2017). Adjustment of the Arabidopsis circadian oscillator by sugar signalling dictates the regulation of starch metabolism. Sci. Rep. 7: 8305.

Shimazaki, K., Doi, M., Assmann, S.M., and Kinoshita, T. (2007). Light regulation of stomatal movement. Annu. Rev. Plant Biol. 58: 219–247.

Shimazaki, K., Terada, J., Tanaka, K., and Kondo, N. (1989). Calvin-Benson cycle enzymes in guard-cell protoplasts from *Vicia faba* L. Implications for the greater utilization of phosphoglycerate/dihydroxyacetone phosphate shuttle between chloroplasts and the cytosol. Plant Physiol. 90: 1057–1064.

Somers, D.E., Webb, A.A.R., Pearson, M., and Kay, S.A. (1998). The short-period mutant, *toc1-1*, alters circadian clock regulation of multiple outputs throughout development in *Arabidopsis thaliana*. Development 125: 485–494.

Sothern, R.B., Tseng, T.-S., Orcutt, S.L., Olszewski, N.E., and Koukkari, W.L. (2002). *GIGANTEA* and *SPINDLY* genes linked to the clock pathway that controls circadian characteristics of transpiration in *Arabidopsis*. Chronobiol. Int. 19: 1005–1022.

Stadler, R., Büttner, M., Ache, P., Hedrich, R., Ivashikina, N., Melzer, M., Shearson, S.M., Smith, S.M., and Sauer, N. (2003). Diurnal and light-regulated expression of AtSTP1 in guard cells of Arabidopsis. Plant Physiol. 133: 528–537.

Stettler, M., Eicke, S., Mettler, T., Messerli, G., Hörtensteiner, S., and Zeeman, S.C. (2009). Blocking the metabolism of starch breakdown products in *Arabidopsis* leaves triggers chloroplast degradation. Mol. Plant 2: 1233–1246.

Stitt, M. and Zeeman, S.C. (2012). Starch turnover: pathways, regulation and role in growth. Curr. Opin. Plant Biol. 15: 282–292.

Streb, S., Delatte, T., Umhang, M., Eicke, S., Schorderet, M., Reinhardt, D., and Zeeman, S.C. (2008). Starch granule biosynthesis in *Arabidopsis* is abolished by removal of all debranching enzymes but restored by the subsequent removal of an endoamylase. Plant Cell 20: 3448–3466.

Streb, S. and Zeeman, S.C. (2012). Starch metabolism in Arabidopsis. Arab. Book 10: e0160.

Sun, Y., Harpazi, B., Wijerathna-Yapa, A., Merilo, E., de Vries, J., Michaeli, D., Gal, M., Cuming, A.C., Kollist, H., and Mosquna, A. (2019). A ligand-independent origin of abscisic acid perception. Proc. Natl. Acad. Sci. U. S. A. 116: 24892–24899.

Tsai, H.-L., Lue, W.-L., Lu, K.-J., Hsieh, M.-H., Wang, S.-M., and Chen, J. (2009). Starch synthesis in Arabidopsis is achieved by spatial cotranscription of core starch metabolism genes. Plant Physiol. 151: 1582–1595.

Vialet-Chabrand, S.R.M., Matthews, J.S.A., McAusland, L., Blatt, M.R., Griffiths, H., and Lawson, T. (2017). Temporal dynamics of stomatal behavior: modeling and implications for photosynthesis and water use. Plant Physiol. 174: 603–613.

Wahl, V., Ponnu, J., Schlereth, A., Arrivault, S., Langenecker, T., Franke, A., Feil, R., Lunn, J.E., Stitt, M., and Schmid, M. (2013). Regulation of flowering by trehalose-6-phosphate signaling in *Arabidopsis thaliana*. Science 339: 704–707.

Wang, Y., Noguchi, K., Ono, N., Inoue, S., Terashima, I., and Kinoshita, T. (2014). Overexpression of plasma membrane H^+-ATPase in guard cells promotes light-induced stomatal opening and enhances plant growth. Proc. Natl. Acad. Sci. U. S. A. 111: 533–538.

Wattebled, F., Dong, Y., Dumez, S., Delvallé, D., Planchot, V., Berbezy, P., Vyas, D., Colonna, P., Chatterjee, M., Ball, S., and D'Hulst, C. (2005). Mutants of Arabidopsis lacking a chloroplastic isoamylase accumulate phytoglycogen and an abnormal form of amylopectin. Plant Physiol. 138: 184–195.

Weise, S.E., Kim, K.S., Stewart, R.P., and Sharkey, T.D. (2005). *β*-maltose is the metabolically active anomer of maltose during transitory starch degradation. Plant Physiol. 137: 756–761.

Weise, S.E., Weber, A.P.M., and Sharkey, T.D. (2004). Maltose is the major form of carbon exported from the chloroplast at night. Planta 218: 474–482.

Westermark, P.O. and Herzel, H. (2013). Mechanism for 12 hr rhythm generation by the circadian clock. Cell Rep. 3: 1228–1238.

Yu, T.-S. et al. (2001). The Arabidopsis *sex1* mutant is defective in the R1 protein, a general regulator of starch degradation in plants, and not in the chloroplast hexose transporter. Plant Cell 13: 1907–1918.

Yu, T.-S. et al. (2005). α-amylase is not required for breakdown of transitory starch in *Arabidopsis* leaves. J. Biol. Chem. 280: 9773–9779.

Yu, T.-S., Lue, W.-L., Wang, S.-M., and Chen, J. (2000). Mutation of Arabidopsis plastid phosphoglucose isomerase affects leaf starch synthesis and floral initiation. Plant Physiol. 123: 319–326.

Zhang, J., de Oliveira Ceciliato, P., Takahashi, Y., Schulze, S., Dubeaux, G., Hauser, F., Azoulay-Shemer, T., Tõldsepp, K., Kollist, H., Rappel, W.-J., and Schroeder, J.I. (2018). Insights into the molecular mechanisms of CO_2-mediated regulation of stomatal movements. Curr. Biol. 28: R1356–R1363.

FIGURE LEGENDS

Figure 1. Characterization of the starch patterns in the starch mutants. **(A)** Schematic view of the pathway of transitory starch in Arabidopsis leaves (adapted from Stitt and Zeeman, 2012; Santelia and Lunn, 2017). In mesophyll cells, starch (yellow shape) is synthetized in the chloroplast (green shape) during the day (left) and broken down at night (right), while it is slightly out of phase in the guard cells. Steps that are specific to the guard cells are depicted by a stomata symbol, but the function of many of the other proteins in the guard cells has not been yet documented. Note that BAM3 is specific to the mesophyll, and that BAM1 can compensate for its absence. Steps that are likely to be minor are indicated in grey, dashed arrows. Uncertain chloroplastic transporters are indicated with a question mark. **(B)** Leaf starch content determined at the end of the day and night periods in control conditions. Error bars are means ± SE. Letters denote significant differences after a Kruskal-Wallis test (α = 5%) followed by multiple comparisons of ranks. **(C)** and **(D)** Iodine staining of starch on entire leaves **(C)** or individual guard cells **(D)** at the end of the day (top rows) or night (bottom rows). The dagger in Col-0†, *ss4*† and *isa1*† indicates that these lines harbour a luciferase reporter that was not used in this study (Methods).

Figure 2. Using a phenotyping pipeline to analyse the diel transpiration in the wild type and two extreme starch mutants, *pgm* and *sex1*. **(A)** Overview of the Phenopsis chamber showing the automaton and the plants with soil covered with cellophane to prevent evaporation as well as a black grid to facilitate plant detection through image analysis (left), close-up above the plant surface featuring the zenithal camera for leaf area determination (top right), and close-up below the pots on the underlying mobile scale (bottom right) that periodically collected the weight data used to feed the PhenoLeaks pipeline for transpiration analysis. **(B)** Leaf starch content determined at the end of the day and night periods in Col-0 for different environmental conditions during the kinetics hereinafter. Error bars are means ± SE. Letters denote significant differences after a Kruskal-Wallis test (α = 5%) followed by multiple comparisons of ranks. **(C)** and **(D)** Diel dynamics of transpiration rate (denoted E) of the wild type Col-0 compared to the starch-free *pgm* **(C)** and the starch-excess *sex1* **(D)** over 2.75 d of control conditions (400 ppm CO_2, 180 µmol m^{-2} s^{-1} irradiance), 1 d of elevated CO_2 (800 ppm in the daytime), 1 d of low irradiance (50 µmol m^{-2} s^{-1} in the daytime), and 2 d

of recovery in control conditions. The white and grey background depict the day (12 h) and night (12 h) periods, respectively. The colour-shaded areas around the mean lines represent the means ± SE.

Figure 3. Quantitative analysis of the transpiration dynamics in Col-0, *pgm* and *sex1*. **(A)** Graphical example of the extraction of parameters on measured data, based on an individual plant of Col-0 in control conditions. For clarity, different parameters have been depicted on different days, but the initial 2.75 d were first averaged into a single 24-h kinetics, from which the parameters were then extracted. The parameters are detailed in the Methods section. **(B)** to **(G)** Boxplots of selected parameters extracted from the measured data for the different genotypes and environments: **(B)** rapid stomatal opening at the day-to-night transition ($A_{rapid\ op}$), **(C)** rapid stomatal closure at the night-to-day transition ($A_{rapid\ clo}$), **(D)** time of maximal daytime transpiration ($t_{day\ max}$), **(E)** time of minimal nighttime transpiration ($t_{night\ min}$), **(F)** cumulative afternoon preclosure after $t_{day\ max}$ (Σ_{preclo}) and **(G)** cumulative nighttime preopening after $t_{night\ min}$ (Σ_{preop}). For each parameter, a two-way mixed ANOVA was done and the effect sizes (η^2_g) of the genotype (G), of the environment (E) and of their interaction (G×E), as well as their respective significance level, are reported above each corresponding plot. Pairwise t-tests were systematically done to assess the differences between genotypes in a given environment, and the differences are reported on the plot when significant. Significance codes are as follows: ^{ns}, not significant; *, $0.05 \leq p_{val} < 10^{-2}$; **, $10^{-2} \leq p_{val} < 10^{-3}$; ***, $10^{-3} \leq p_{val} < 10^{-4}$; ****, $10^{-4} \leq p_{val}$.

Figure 4. Modelling diel transpiration dynamics and obtaining associated parameters in Col-0, *pgm* and *sex1*. **(A)** Structure of the sinusoidal model, graphical example of the resulting curve ($\hat{E}$, black line) and illustration of each component (coloured lines) using the set of parameters fitted to the data (black points) of the same Col-0 individual plant as shown in Figure 1C. **(B)** Graphical example of the extraction of quantitative parameters on fitted data, similar as for Figure 1C, using the same individual plant. **(C)** to **(H)** Boxplots of fitted parameters for the different genotypes and environments: **(C)** Mean transpiration rate over a 24 h period (E_{mean}), **(D)** semi-amplitude of the square wave (A_{SQW}), **(E)** semi-amplitude of the fundamental sine wave (A_1), **(F)** semi-amplitude

of the second harmonic (A_2), **(G)** phase of the fundamental sine wave (φ_1) and **(H)** phase of the second harmonic (φ_2). **(I)** and **(J)** Boxplots of selected parameters extracted from the fitted data for the different genotypes and environments: **(I)** cumulative afternoon preclosure ($\widehat{\Sigma}_{preclo}$) and **(J)** cumulative nighttime preopening ($\widehat{\Sigma}_{preop}$). Significance codes for ANOVA effect sizes (η^2_g) and pairwise t-tests are like those in Figure 3.

Figure 5. Heatmap of the parameters extracted from, or fitted to, the diel transpiration dynamics. Scaled and centred data from the whole experiment (17 genotypes $\times$ 5 environments) were used. Hierarchical clustering analysis was performed on the treatments (left) and on the parameters (top) and each dendrogram was graphically split into four groups for sake of clarity. For each line, the environment is depicted by the colour of the cell next to the treatment dendrogram, while the genotype is indicated on the right of the heatmap. The dagger in Col-0†, *ss4*† and *isa1*† indicates that these lines harbour a luciferase reporter that was not used in this study (Methods). Note that *abcb14*-1 and -2 are not starch mutants (Methods). The parameters are the ones presented in Figures 3A, 4A, 4B.

Figure 6. Analysis of diel transpiration of *isa1* and *ss4*, two mutants of the starch biosynthesis pathway. **(A)** and **(B)** Diel dynamics of transpiration rate of the wild type Col-0 compared to *isa1* **(A)** and *ss4* **(B)** in the same conditions as in Figure 2. The colour-shaded areas around the mean lines represent the means ± SE. **(C)** to **(H)** Boxplots of fitted parameters for the different genotypes and environments: **(C)** E_{mean}, **(D)** A_{SQW}, **(E)** A_1, **(F)** A_2, **(G)** φ_1 and **(H)** φ_2. **(I)** and **(J)** Boxplots of selected parameters extracted from the measured data for the different genotypes and environments: **(I)** Σ_{preclo} and **(J)** Σ_{preop}. Abbreviations for parameters and significance codes for ANOVA effect sizes (η^2_g) and pairwise t-tests are like those in Figures 3 and 4. The dagger in Col-0†, *ss4*† and *isa1*† indicates that these lines harbour a luciferase reporter that was not used in this study (Methods).

Figure 7. Analysis of diel transpiration of *mex1*, *dpe1* and *dpe2*, three mutants of the starch breakdown pathway. **(A)** to **(C)** Diel dynamics of transpiration rate of the wild type Col-0 compared to *mex1* **(A)**, *dpe1* **(B)** and *dpe2* **(C)** in the same conditions as in Figure

2. The colour-shaded areas around the mean lines represent the means ± SE. **(D)** to **(I)** Boxplots of fitted parameters: **(D)** E_{mean}, **(E)** A_{SQW}, **(F)** A_1, **(G)** A_2, **(H)** φ_1 and **(I)** φ_2. **(J)** and **(K)** Boxplots of selected parameters extracted from the measured data: **(J)** Σ_{preclo} and **(K)** Σ_{preop}. Abbreviations for parameters and significance codes for ANOVA effect sizes (η^2_g) and pairwise t-tests are like those in Figures 3 and 4.

Figure 8. Analysis of diel transpiration of *pgi*, *amy3 bam1* and *bam1 bam3*, three mutants with contrasting starch metabolism in different tissues. **(A)** to **(C)** Diel dynamics of transpiration rate of the wild type Col-0 compared to *pgi* **(A)**, *amy3 bam1* **(B)** and *bam1 bam3* **(C)** in the same conditions as in Figure 2. The colour-shaded areas around the mean lines represent the means ± SE. **(D)** to **(I)** Boxplots of fitted parameters: **(D)** E_{mean}, **(E)** A_{SQW}, **(F)** A_1, **(G)** A_2, **(H)** φ_1 and **(I)** φ_2. **(J)** and **(K)** Boxplots of selected parameters extracted from the measured data: **(J)** Σ_{preclo} and **(K)** Σ_{preop}. Abbreviations for parameters and significance codes for ANOVA effect sizes (η^2_g) and pairwise t-tests are like those in Figures 3 and 4.

Figure 9. Analysis of diel transpiration of *abcb14*-1 and *abcb14*-2. **(A)** and **(B)** Diel dynamics of transpiration rate of the wild type Col-0 compared to *abcb14*-1 **(A)** and *abcb14*-2 **(B)** in the same conditions as in Figure 2. The colour-shaded areas around the mean lines represent the means ± SE. **(C)** to **(H)** Boxplots of fitted parameters: **(C)** E_{mean}, **(D)** A_{SQW}, **(E)** A_1, **(F)** A_2, **(G)** φ_1 and **(H)** φ_2. **(I)** and **(J)** Boxplots of selected parameters extracted from the measured data: **(I)** Σ_{preclo} and **(J)** Σ_{preop}. Abbreviations for parameters and significance codes for ANOVA effect sizes (η^2_g) and pairwise t-tests are like those in Figures 3 and 4.

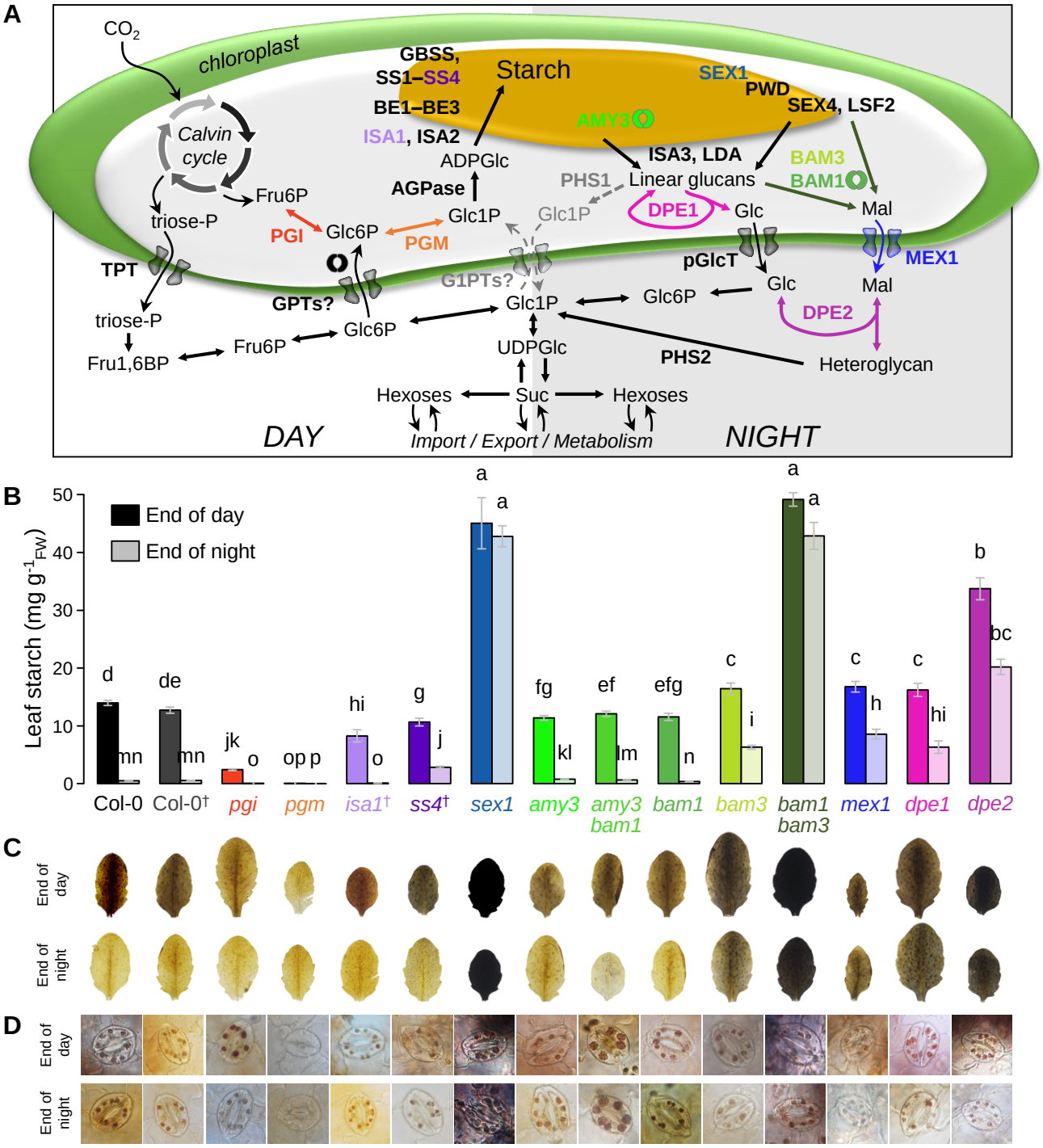

Figure 1. Characterization of the starch patterns in the starch mutants. **(A)** Schematic view of the pathway of transitory starch in Arabidopsis leaves (adapted from Stitt and Zeeman, 2012; Santelia and Lunn, 2017). In mesophyll cells, starch (yellow shape) is synthetized in the chloroplast (green shape) during the day (left) and broken down at night (right), while it is slightly out of phase in the guard cells. Steps that are specific to the guard cells are depicted by a stomata symbol, but the function of many of the other proteins in the guard cells has not been yet documented. Note that BAM3 is specific to the mesophyll, and that BAM1 can compensate for its absence. Steps that are likely to be minor are indicated in grey, dashed arrows. Uncertain chloroplastic transporters are indicated with a question mark. **(B)** Leaf starch content determined at the end of the day and night periods in control conditions. Error bars are means ± SE (n = 4). Letters denote significant differences after a Kruskal-Wallis test (α = 5%) followed by multiple comparisons of ranks. **(C)** and **(D)** Iodine staining of starch on entire leaves **(C)** or individual guard cells **(D)** at the end of the day (top rows) or night (bottom rows). The dagger in Col-0†, *ss4*† and *isa1*† indicates that these lines harbour a luciferase reporter that was not used in this study (Methods).

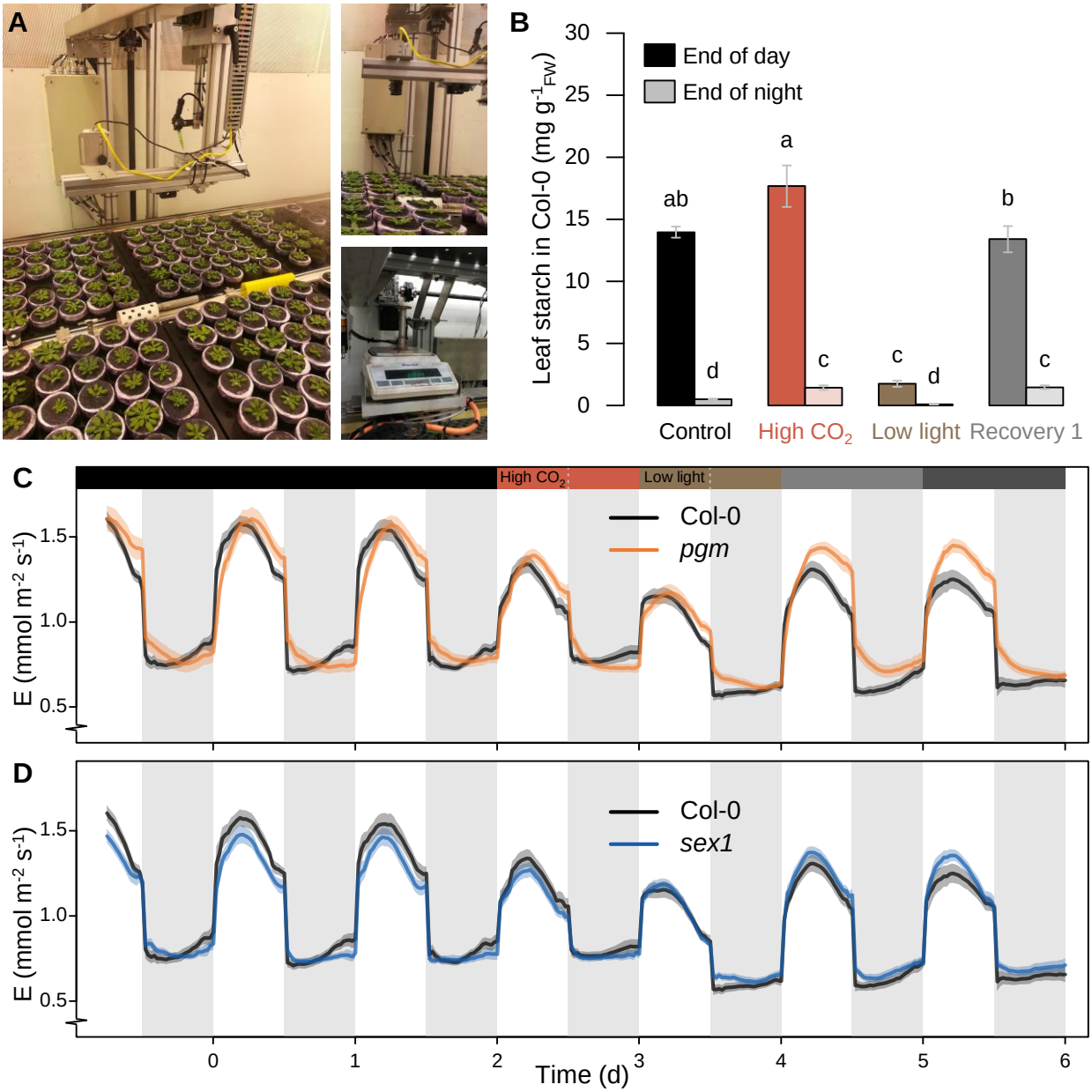

Figure 2. Using a phenotyping pipeline to analyse the diel transpiration in the wild type and two extreme starch mutants, *pgm* and *sex1*. **(A)** Overview of the Phenopsis chamber showing the automaton and the plants with soil covered with cellophane to prevent evaporation as well as a black grid to facilitate plant detection through image analysis (left), close-up above the plant surface featuring the zenithal camera for leaf area determination (top right), and close-up below the pots on the underlying mobile scale (bottom right) that periodically collected the weight data used to feed the PhenoLeaks pipeline for transpiration analysis. **(B)** Leaf starch content determined at the end of the day and night periods in Col-0 for different environmental conditions during the kinetics hereinafter. Error bars are means ± SE. Letters denote significant differences after a Kruskal-Wallis test (α = 5%) followed by multiple comparisons of ranks. **(C)** and **(D)** Diel dynamics of transpiration rate (denoted E) of the wild type Col-0 compared to the starch-free *pgm* **(C)** and the starch-excess *sex1* **(D)** over 2.75 d of control conditions (400 ppm CO_2, 180 µmol m^{-2} s^{-1} irradiance), 1 d of elevated CO_2 (800 ppm in the daytime), 1 d of low irradiance (50 µmol m^{-2} s^{-1} in the daytime), and 2 d of recovery in control conditions. The white and grey background depict the day (12 h) and night (12 h) periods, respectively. The colour-shaded areas around the mean lines represent the means ± SE.

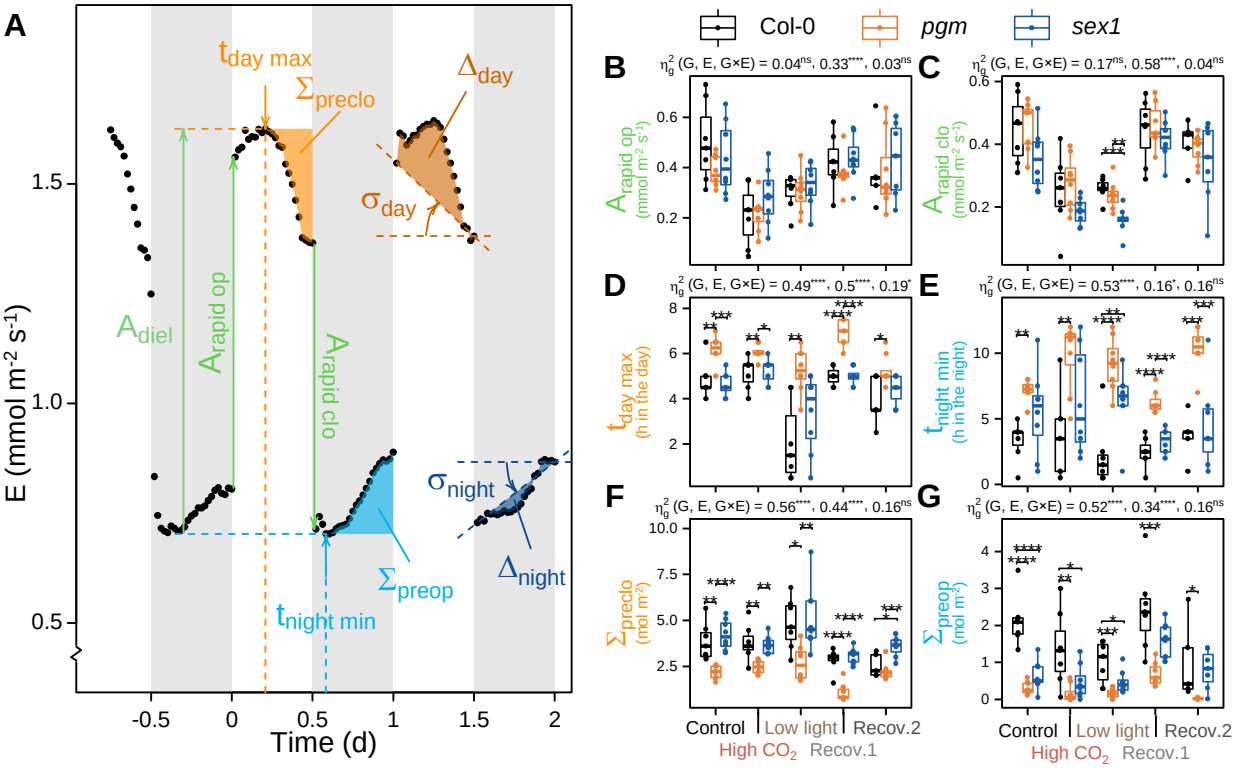

Figure 3. Quantitative analysis of the transpiration dynamics in Col-0, *pgm* and *sex1*. **(A)** Graphical example of the extraction of parameters on measured data, based on an individual plant of Col-0 in control conditions. For clarity, different parameters have been depicted on different days, but the initial 2.75 d were first averaged into a single 24-h kinetics, from which the parameters were then extracted. The parameters are detailed in the Methods section. **(B)** to **(G)** Boxplots of selected parameters extracted from the measured data for the different genotypes and environments: **(B)** rapid stomatal opening at the day-to-night transition ($A_{rapid\ op}$), **(C)** rapid stomatal closure at the night-to-day transition ($A_{rapid\ clo}$), **(D)** time of maximal daytime transpiration ($t_{day\ max}$), **(E)** time of minimal nighttime transpiration ($t_{night\ min}$), **(F)** cumulative afternoon preclosure after $t_{day\ max}$ (Σ_{preclo}) and **(G)** cumulative nighttime preopening after $t_{night\ min}$ (Σ_{preop}). For each parameter, a two-way mixed ANOVA was done and the effect sizes (η^2_g) of the genotype (G), of the environment (E) and of their interaction (G×E), as well as their respective significance level, are reported above each corresponding plot. Pairwise t-tests were systematically done to assess the differences between genotypes in a given environment, and the differences are reported on the plot when significant. Significance codes are as follows: ^{ns}, not significant; *, $0.05 \leq p_{val} < 10^{-2}$; **, $10^{-2} \leq p_{val} < 10^{-3}$; ***, $10^{-3} \leq p_{val} < 10^{-4}$; ****, $10^{-4} \leq p_{val}$.

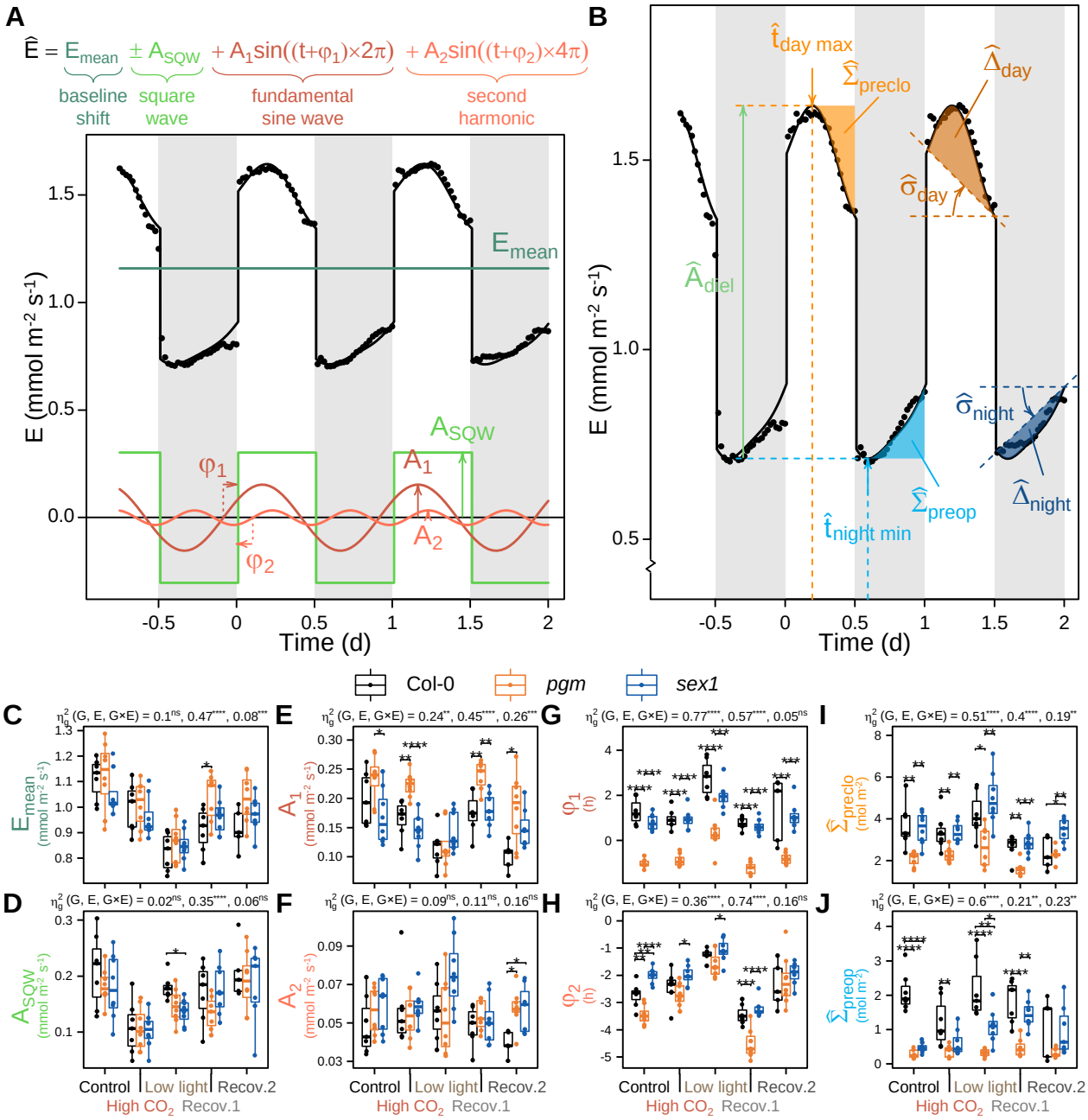

Figure 4. Modelling diel transpiration dynamics and obtaining associated parameters in Col-0, *pgm* and *sex1*. **(A)** Structure of the sinusoidal model, graphical example of the resulting curve ($\hat{E}$, black line) and illustration of each component (coloured lines) using the set of parameters fitted to the data (black points) of the same Col-0 individual plant as shown in Figure 1C. **(B)** Graphical example of the extraction of quantitative parameters on fitted data, similar as for Figure 1C, using the same individual plant. **(C)** to **(H)** Boxplots of fitted parameters for the different genotypes and environments: **(C)** Mean transpiration rate over a 24 h period (E_{mean}), **(D)** semi-amplitude of the square wave (A_{SQW}), **(E)** semi-amplitude of the fundamental sine wave (A_1), **(F)** semi-amplitude of the second harmonic (A_2), **(G)** phase of the fundamental sine wave (φ_1) and **(H)** phase of the second harmonic (φ_2). **(I)** and **(J)** Boxplots of selected parameters extracted from the fitted data for the different genotypes and environments: **(I)** cumulative afternoon preclosure ($\hat{\Sigma}_{preclo}$) and **(J)** cumulative nighttime preopening ($\hat{\Sigma}_{preop}$). Significance codes for ANOVA effect sizes (η^2_g) and pairwise t-tests are like those in Figure 3.

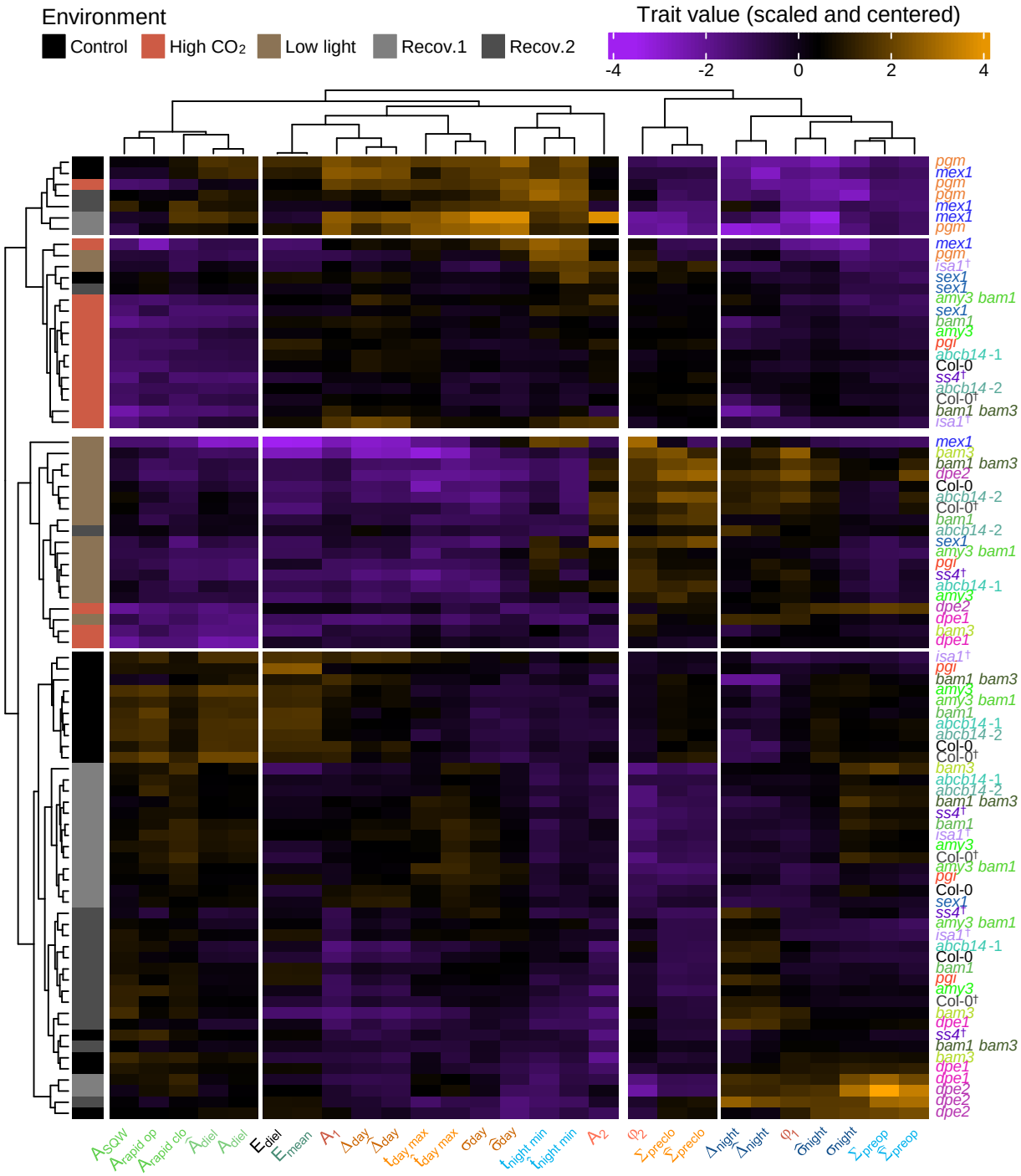

Figure 5. Heatmap of the parameters extracted from, or fitted to, the diel transpiration dynamics. Scaled and centred data from the whole experiment (17 genotypes × 5 environments) were used. Hierarchical clustering analysis was performed on the treatments (left) and on the parameters (top) and each dendrogram was graphically split into four groups for sake of clarity. For each line, the environment is depicted by the colour of the cell next to the treatment dendrogram, while the genotype is indicated on the right of the heatmap. The dagger in Col-0†, *ss4*† and *isa1*† indicates that these lines harbour a luciferase reporter that was not used in this study (Methods). Note that *abcb14*-1 and -2 are not starch mutants (Methods). The parameters are the ones presented in Figures 3A, 4A, 4B.

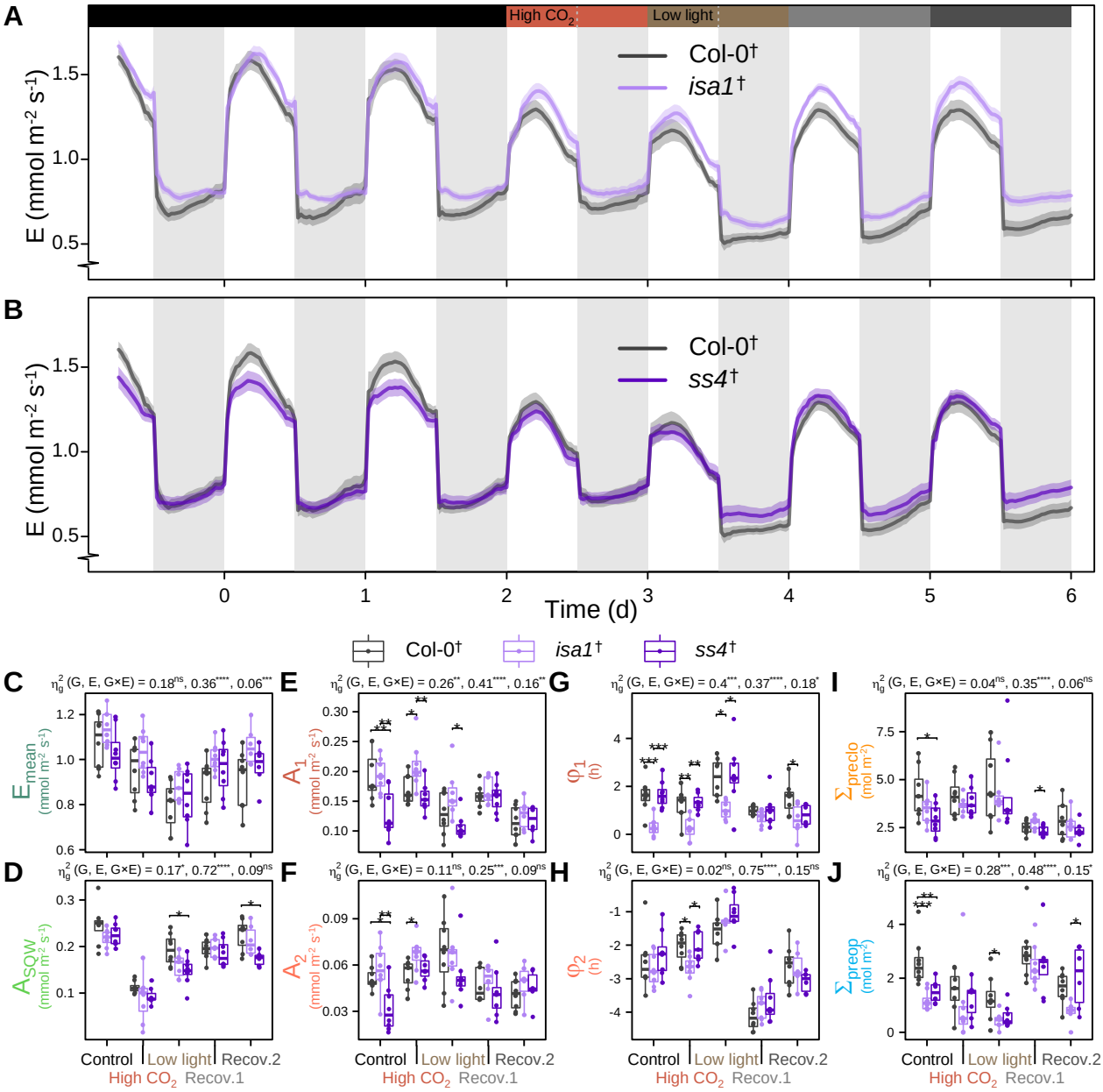

Figure 6. Analysis of diel transpiration of *isa1* and *ss4*, two mutants of the starch biosynthesis pathway. **(A)** and **(B)** Diel dynamics of transpiration rate of the wild type Col-0 compared to *isa1* **(A)** and *ss4* **(B)** in the same conditions as in Figure 2. The colour-shaded areas around the mean lines represent the means ± SE. **(C)** to **(H)** Boxplots of fitted parameters for the different genotypes and environments: **(C)** E_{mean}, **(D)** A_{SQW}, **(E)** A_1, **(F)** A_2, **(G)** φ_1 and **(H)** φ_2. **(I)** and **(J)** Boxplots of selected parameters extracted from the measured data for the different genotypes and environments: **(I)** Σ_{preclo} and **(J)** Σ_{preop}. Abbreviations for parameters and significance codes for ANOVA effect sizes (η^2_g) and pairwise t-tests are like those in Figures 3 and 4. The dagger in Col-0†, *ss4*† and *isa1*† indicates that these lines harbour a luciferase reporter that was not used in this study (Methods).

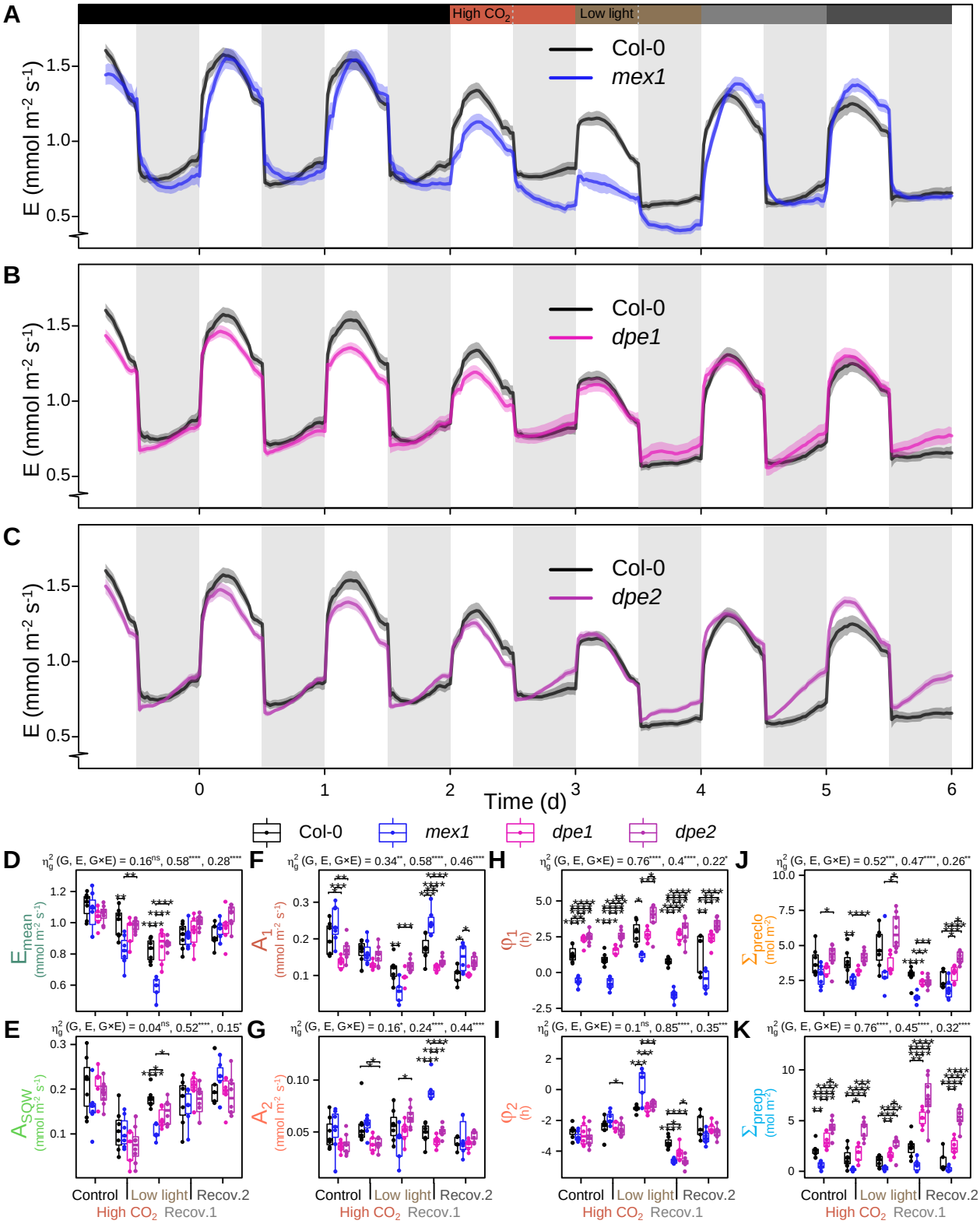

Figure 7. Analysis of diel transpiration of *mex1*, *dpe1* and *dpe2*, three mutants of the starch breakdown pathway. **(A)** to **(C)** Diel dynamics of transpiration rate of the wild type Col-0 compared to *mex1* **(A)**, *dpe1* **(B)** and *dpe2* **(C)** in the same conditions as in Figure 2. The colour-shaded areas around the mean lines represent the means ± SE. **(D)** to **(I)** Boxplots of fitted parameters: **(D)** E_{mean}, **(E)** A_{SQW}, **(F)** A_1, **(G)** A_2, **(H)** φ_1 and **(I)** φ_2. **(J)** and **(K)** Boxplots of selected parameters extracted from the measured data: **(J)** Σ_{preclo} and **(K)** Σ_{preop}. Abbreviations for parameters and significance codes for ANOVA effect sizes (η^2_g) and pairwise t-tests are like those in Figures 3 and 4.

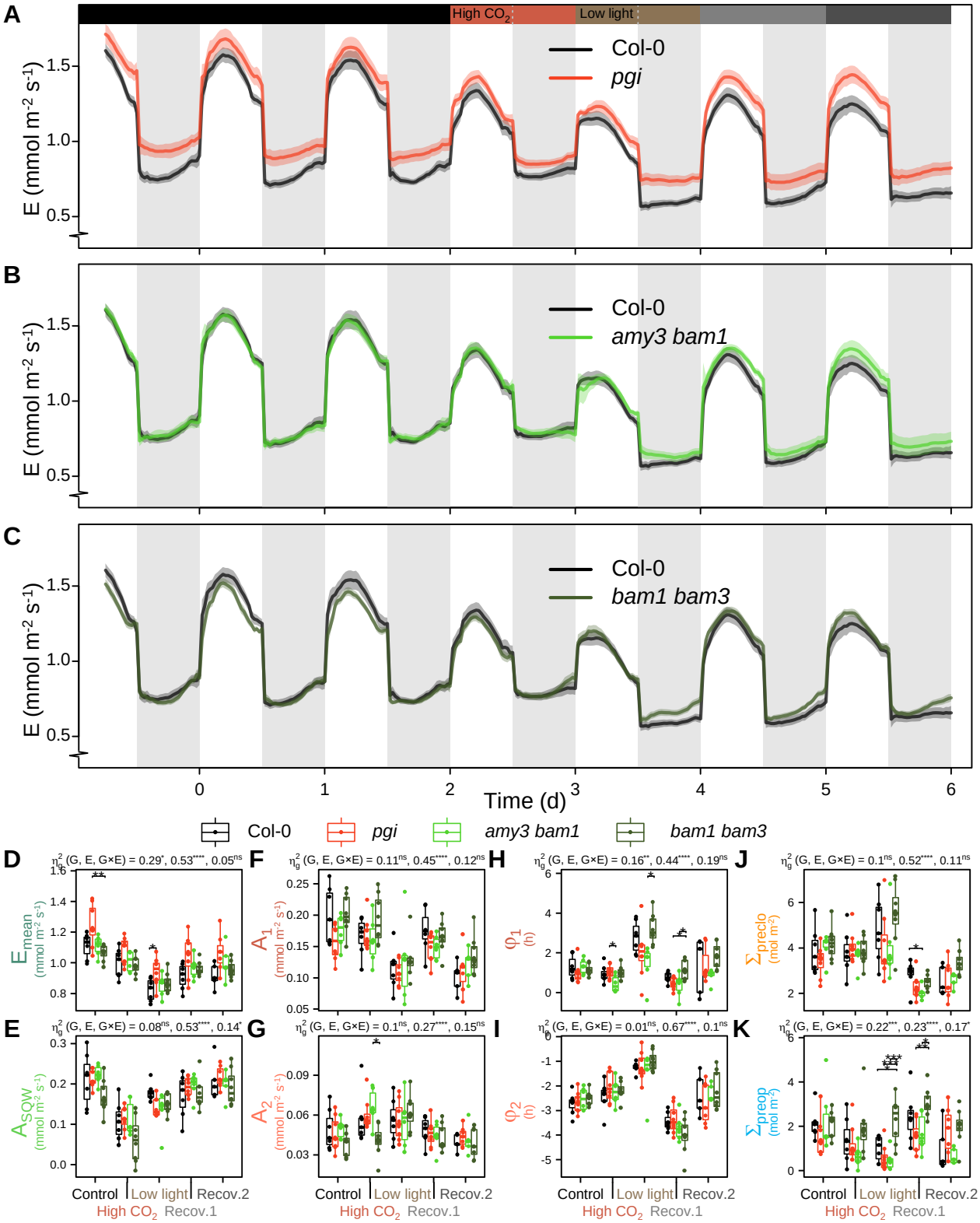

Figure 8. Analysis of diel transpiration of *pgi*, *amy3 bam1* and *bam1 bam3*, three mutants with contrasting starch metabolism in different tissues. **(A)** to **(C)** Diel dynamics of transpiration rate of the wild type Col-0 compared to *pgi* **(A)**, *amy3 bam1* **(B)** and *bam1 bam3* **(C)** in the same conditions as in Figure 2. The colour-shaded areas around the mean lines represent the means ± SE. **(D)** to **(I)** Boxplots of fitted parameters: **(D)** E_{mean}, **(E)** A_{SQW}, **(F)** A_1, **(G)** A_2, **(H)** φ_1 and **(I)** φ_2. **(J)** and **(K)** Boxplots of selected parameters extracted from the measured data: **(J)** Σ_{preclo} and **(K)** Σ_{preop}. Abbreviations for parameters and significance codes for ANOVA effect sizes (η^2_g) and pairwise t-tests are like those in Figures 3 and 4.

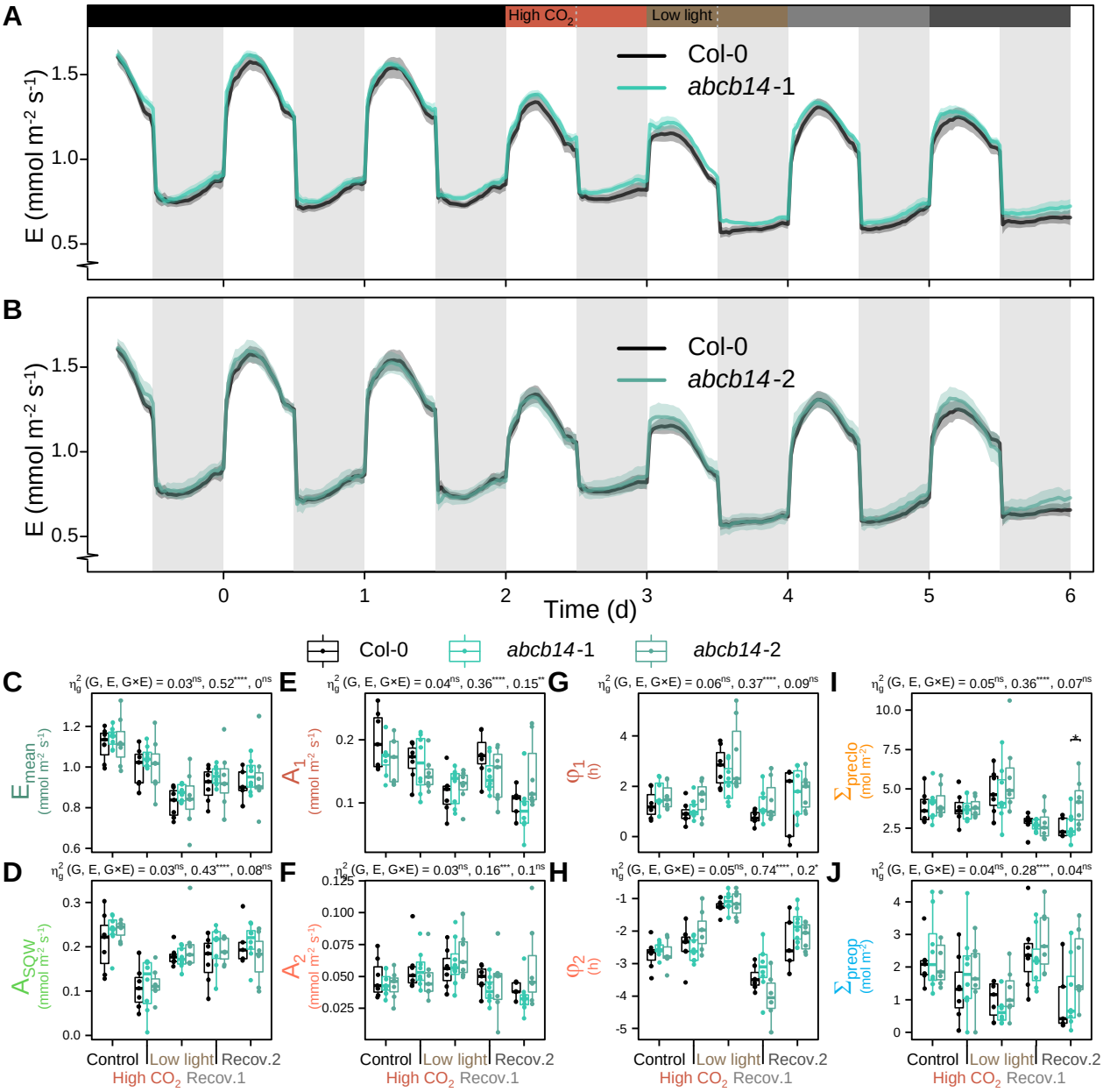

Figure 9. Analysis of diel transpiration of *abcb14*-1 and *abcb14*-2. **(A)** and **(B)** Diel dynamics of transpiration rate of the wild type Col-0 compared to *abcb14*-1 **(A)** and *abcb14*-2 **(B)** in the same conditions as in Figure 2. The colour-shaded areas around the mean lines represent the means ± SE. **(C)** to **(H)** Boxplots of fitted parameters: **(C)** E_{mean}, **(D)** A_{SQW}, **(E)** A_1, **(F)** A_2, **(G)** φ_1 and **(H)** φ_2. **(I)** and **(J)** Boxplots of selected parameters extracted from the measured data: **(I)** Σ_{preclo} and **(J)** Σ_{preop}. Abbreviations for parameters and significance codes for ANOVA effect sizes (η^2_g) and pairwise t-tests are like those in Figures 3 and 4.